

# Axial couplings in heavy hadron chiral perturbation theory at the next-to-leading order

William Detmold<sup>a,b</sup>, C.-J. David Lin<sup>c,d</sup>, Stefan Meinel<sup>a</sup>

<sup>a</sup> *Department of Physics, College of William and Mary, Williamsburg, VA 23187-8795, USA*

<sup>b</sup> *Jefferson Laboratory, 12000 Jefferson Avenue, Newport News, VA 23606, USA*

<sup>c</sup> *Institute of Physics, National Chiao-Tung University, Ta-Hsueh Road, Hsinchu 300, Taiwan*

<sup>d</sup> *Division of Physics, National Centre for Theoretical Sciences, Kuang-Fu Road, Hsinchu 300, Taiwan*

## Abstract:

We present calculations of axial-current matrix elements between various heavy-meson and heavy-baryon states to the next-to-leading order in heavy hadron chiral perturbation theory in the  $p$ -regime. When compared with data from lattice computations or experiments, these results can be used to determine the axial couplings in the chiral Lagrangian. Our calculation is performed in partially-quenched chiral perturbation theory for both SU(4|2) and SU(6|3). We incorporate finite-size effects arising from a single Goldstone meson wrapping around the spatial volume. Results for full QCD with two and three flavours can be obtained straightforwardly by taking the sea-quark masses to be equal to the valence-quark masses. To illustrate the impact of our chiral perturbation theory calculation on lattice computations, we analyse the SU(2) full QCD results in detail. We also study one-loop contributions relevant to the heavy hadron strong-decay amplitudes involving final-state Goldstone bosons, and demonstrate that the quark-mass dependence of these amplitudes can be significantly different from that of the axial current matrix elements containing only single hadron external states.

PACS numbers: 12.38.Gc, 12.39.Fe, 12.39.Hg, 14.20.Mr, 14.40.Nd

## I. INTRODUCTION

The physics of  $b$  hadrons is an important and active field of research, both experimentally and theoretically.  $B$  mesons have played an important role in our understanding of flavour physics in the Standard Model (SM) and its possible extension. The on-going LHCb experiment and possible future  $B$  factories will produce significantly improved experimental information for  $B$  mesons which will, in turn, lead to better constraints on the relevant SM parameters or reveal deviations from the SM. In addition, a large amount of polarised single-bottom baryon data will be produced. This will allow extensive studies of the spectrum and the decays of these baryons. Since the baryons carry different spin quantum numbers, they may offer additional opportunities for probing the coupling structure of physics beyond the SM. In performing such investigations, it is necessary to compare experimental results to precise theoretical calculations in which non-perturbative strong-interaction effects are well controlled. This is becoming achievable because of the progress in Lattice QCD.

Calculations in Lattice QCD are often performed at unphysical light-quark masses due to the limited computing resources. In order to obtain high-precision theoretical predictions for spectral quantities and matrix elements, it is essential to use chiral perturbation theory ( $\chi$ PT) to extrapolate to the physical quark masses. For systems of hadrons containing a single valence  $b$  or  $\bar{b}$  quark, the relevant chiral effective field theory is heavy-hadron  $\chi$ PT (HH $\chi$ PT) [1–5]. In addition to the low-energy constants in the chiral Lagrangian of the Goldstone boson sector, there are three unknown coupling constants in this effective theory at the leading order (LO). These constants, defined explicitly as  $g_{1,2,3}$  in Eq. (24) in Sec. II, accompany axial couplings of heavy hadrons to the Goldstone boson sector and appear in all chiral extrapolations using HH $\chi$ PT. Therefore, the accurate determination of  $g_{1,2,3}$  is one of the most important tasks in the Lattice QCD calculations for  $b$ -physics phenomenology.

In this work, we compute the matrix elements of the quark-level axial currents,

$$\mathcal{J}_{ud,\mu} = \bar{d}\gamma_\mu\gamma_5 u, \text{ and } \mathcal{J}_{us,\mu} = \bar{s}\gamma_\mu\gamma_5 u, \quad (1)$$

between various heavy-light meson and single- $b$  baryon states to the next-to-leading order (NLO) in HH $\chi$ PT. In particular, we calculate the relevant one-loop contributions to these matrix elements. When compared with data from lattice calculations or experiments, our results can be used to extract the above-mentioned three axial couplings in HH $\chi$ PT. Our calculation is performed in partially-quenched chiral perturbation theory (PQ $\chi$ PT) using the supersymmetric formulation [6], for both SU(4|2) and SU(6|3). The “full-QCD” limit can be taken straightforwardly from our results by setting the sea-quark masses to be equal to the valence-quark masses. Our one-loop computation is carried out for finite spatial volume in the  $p$ -regime<sup>1</sup>, following the same method as in Refs. [9, 10]. As pointed out in Ref. [11], in heavy-light meson systems, finite-volume effects arising from higher-order terms in the chiral expansion can be estimated. This requires high-precision information on the  $B^*-B-\pi$  coupling beyond that which is currently available. Nevertheless, such higher-order effects are insignificant for current and future lattice calculations, since computations with small pion masses in large volumes are becoming standard.

In this paper, we present our results in the isospin limit. However, in the case of SU(6|3), we include the SU(3) breaking<sup>2</sup> effects, both in the external states and in the axial currents. At NLO in HH $\chi$ PT, the axial-current matrix elements for heavy hadrons can be written in the general form

$$g(1 + g^2 L + g'^2 L' + L'') + \text{analytic terms}, \quad (2)$$

where  $g$  and  $g'$  are variously  $g_1$ ,  $g_2$  and  $g_3$  in Eq. (24), and  $L$ ,  $L'$  and  $L''$  are the contributions from one-loop diagrams. The determination of  $g_1$  using lattice QCD has been attempted by various groups [12–17]. However, the correct quark mass dependence (based on the symmetries of QCD) of the axial matrix elements was not previously known. Using the current work, extrapolations to the physical quark masses can be made rigorously.

This paper is organised in the following way. Section II contains an introduction to HH $\chi$ PT. In Sec. III, we first present the general structure of the one-loop contributions to the axial-current matrix elements, before giving the

<sup>1</sup> Studies of the heavy-meson systems in the  $\epsilon$ -regime can be found in Ref. [7, 8].

<sup>2</sup> More precisely, we consider identical SU(3) breaking effects in the sea, valence and ghost sectors of SU(6|3) but for simplicity, refer to this as SU(3) breaking.

results in the case of SU(2) in Sec. IV. Results for SU(4|2) and SU(6|3) HH $\chi$ PT are presented in Sec. V, emphasising the quark flavour flow picture. In Sec. VI, the strong-decay amplitudes involving final-state Goldstone mesons are also computed before we conclude. Technical details of the results are included in the appendices.

## II. HEAVY HADRON CHIRAL PERTURBATION THEORY

The partially quenched (PQ) chiral Lagrangian<sup>3</sup> for the Goldstone mesons is

$$\mathcal{L}_G = \frac{f^2}{8} \text{str} [(\partial_\mu \Sigma^\dagger)(\partial^\mu \Sigma) + \Sigma^\dagger \chi + \chi^\dagger \Sigma] + [\alpha(\partial_\mu \Phi_0)(\partial^\mu \Phi_0) - M_0^2 \Phi_0^2], \quad (3)$$

where  $\Sigma = \exp(2i\Phi/f)$  is the non-linear Goldstone particle field, with  $\Phi$  being the matrix containing the standard Goldstone fields in the quark-flavour basis. We use  $f = 132$  MeV. In this work, we follow the supersymmetric formulation of PQ chiral perturbation theory (PQ $\chi$ PT) [6]. Therefore under SU(4|2)<sub>L</sub>  $\otimes$  SU(4|2)<sub>R</sub> or SU(6|3)<sub>L</sub>  $\otimes$  SU(6|3)<sub>R</sub>,  $\Sigma$  transforms as

$$\Sigma \longrightarrow U_L \Sigma U_R^\dagger, \quad (4)$$

where

$$U_L \in \text{SU}(4|2)_L \text{ or } \text{SU}(6|3)_L,$$

$$U_R \in \text{SU}(4|2)_R \text{ or } \text{SU}(6|3)_R. \quad (5)$$

The symbol ‘‘str’’ in the above equation means ‘‘supertrace’’. The variable  $\chi$  is defined as

$$\chi \equiv 2B_0 \mathcal{M}_q, \quad (6)$$

where  $B_0$  is a low energy constant related to the chiral condensate and, in the isospin limit, the quark mass matrix,  $\mathcal{M}_q$  is

$$\mathcal{M}_q = \text{diag}(\underbrace{m_u, m_u}_{\text{valence}}, \underbrace{m_{u'}, m_{u'}}_{\text{sea}}, \underbrace{m_u, m_u}_{\text{ghost}}), \quad (7)$$

in the SU(4|2) theory, and is

$$\mathcal{M}_q = \text{diag}(\underbrace{m_u, m_u, m_s}_{\text{valence}}, \underbrace{m_{u'}, m_{u'}, m_{s'}}_{\text{sea}}, \underbrace{m_u, m_u, m_s}_{\text{ghost}}), \quad (8)$$

in the SU(6|3) theory. We keep the strange quark mass different from that of the up and down quarks in the valence, sea and ghost sectors. Notice that the flavour singlet state  $\Phi_0 = \text{str}(\Phi)/\sqrt{6}$  is rendered heavy by the  $U(1)_A$  anomaly in PQQCD [19, 20] and can be integrated out, resulting in residual ‘‘hairpin’’ structures.

The inclusion of the heavy-light mesons in chiral perturbation theory was first proposed in Refs. [1–3], with the generalisation to quenched and partially quenched theories given in Ref. [21, 22]. The  $1/M_P$  and chiral corrections were studied by Boyd and Grinstein [23]. The  $B$  and  $B^*$  meson fields appear in this effective theory through the ‘‘superfield’’

$$H_i^{(\bar{b})} = (B_{i,\mu}^* \gamma^\mu - B_i \gamma_5) \frac{1 - \not{p}}{2}, \quad (9)$$

---

<sup>3</sup> In this paper, we only address situations where there are no multi-particle thresholds involved in loops. Therefore, in spite of the sickness pointed out in Ref. [18], we can still use the Minkowski formalism of PQ chiral perturbation theory.

where  $v_\mu$  is the 4-velocity of the meson fields,  $B_i$  and  $B_{i,\mu}^*$  annihilate pseudoscalar and vector mesons containing an anti- $b$  quark<sup>4</sup> and a light quark of flavour  $i$ . Under the heavy-quark spin transformation  $S_h$  and the unbroken light-flavour transformation  $U(x)$ , the field  $H^{(\bar{b})}$  transforms as

$$H_i^{(\bar{b})}(x) \longrightarrow U_i^j(x) H_j^{(\bar{b})}(x) S_h^{-1}. \quad (10)$$

Also, the conjugate field, which creates heavy-light mesons containing an anti- $b$  quark and a light quark of flavour  $i$ , is defined as

$$\bar{H}_i^{(\bar{b})} = \gamma^0 H_i^{(\bar{b})\dagger} \gamma_0, \quad (11)$$

and transforms under  $S_h$  and  $U(x)$  as

$$\bar{H}_i^{(\bar{b})}(x) \longrightarrow S_h \bar{H}_j^{(\bar{b})}(x) (U^\dagger)^j_i(x). \quad (12)$$

The introduction of the single- $b$  baryons to  $\chi$ PT was pioneered by authors of Refs. [3–5], and the effective theory was generalised to the PQ scenario in Ref. [25]. Since the two valence light quarks in such baryons may carry total spin quantum numbers<sup>5</sup>  $s_l = 0$  or  $s_l = 1$ , there are two types of heavy baryons. At the quark level, these two types of baryons carrying light flavours  $i$  and  $j$  are described by the interpolating fields

$$\begin{aligned} \mathcal{T}_{ij}^\gamma &\sim b^{\gamma,c} \left[ q_i^{\alpha,a} q_j^{\beta,b} + q_j^{\beta,b} q_i^{\alpha,a} \right] \epsilon_{abc} (C\gamma_5)_{\alpha\beta} \text{ for } s_l = 0, \\ \mathcal{S}_{ij}^{\gamma,\mu} &\sim b^{\gamma,c} \left[ q_i^{\alpha,a} q_j^{\beta,b} - q_j^{\beta,b} q_i^{\alpha,a} \right] \epsilon_{abc} (C\gamma^\mu)_{\alpha\beta} \text{ for } s_l = 1, \end{aligned} \quad (13)$$

where  $C$  is the charge-conjugation matrix,  $\alpha, \beta$  and  $\gamma$  are the Dirac indices and  $a, b$  and  $c$  are colour indices. In full QCD, the  $\mathcal{T}$  fields are anti-symmetric and the  $\mathcal{S}$  fields are symmetric under the exchange of the light flavour indices. In the PQ theory, the flavour structure of these interpolating fields has the properties

$$\begin{aligned} \mathcal{T}_{ij} &= (-1)^{\eta_i \eta_j} \mathcal{T}_{ji}, \\ \mathcal{S}_{ij}^\mu &= (-1)^{1+\eta_i \eta_j} \mathcal{S}_{ji}^\mu, \end{aligned} \quad (14)$$

where

$$\eta_i = \begin{cases} 1 & \text{when } i \in \text{valence and sea,} \\ 0 & \text{when } i \in \text{ghost,} \end{cases} \quad (15)$$

accounts for different statistics of quarks in PQCD. These fields transform as **39**- and **42**-plets under the SU(6|3) flavour rotation, while they transform as **17**- and **19**-plets under the SU(4|2) flavour rotation. The baryon fields are included in heavy-hadron chiral perturbation theory (HH $\chi$ PT) according to the flavour properties in Eq. (14). In the case of  $N_f = 3$  ( $N_f$  refers to the number of sea-quark flavours), the pure valence-valence sector of the  $s_l = 0$  baryons is related to the physical states of  $\Lambda_b$  and  $\Xi_b^{\pm 1/2}$  via

$$T_{(\text{valence-valence})} = \frac{1}{\sqrt{2}} \begin{pmatrix} 0 & \Lambda_b & \Xi_b^{+1/2} \\ -\Lambda_b & 0 & \Xi_b^{-1/2} \\ -\Xi_b^{+1/2} & -\Xi_b^{-1/2} & 0 \end{pmatrix}, \quad (16)$$

where the superscript indicates the 3-component of the isospin. Since the light-light di-quark is of spin-1 in the  $\mathcal{S}_{ij}^\mu$  fields, such baryons can be in spin 1/2 or 3/2 states which are degenerate in the heavy quark limit. Therefore they are best described by the ‘‘superfield’’

$$S_{ij}^\mu = \sqrt{\frac{1}{3}} (v^\mu + \gamma^\mu) \gamma_5 B_{ij} + B_{ij}^{*\mu}, \quad (17)$$

<sup>4</sup> We follow the standard notation [24] for the flavour content of  $B$  mesons, so that e.g.  $B_u = B^+ = u\bar{b}$ .

<sup>5</sup> The total spin of the light degrees of freedom is a conserved quantum number because of the heavy quark symmetry.

where  $B_{ij}$  and  $B_{ij}^{*\mu}$  are spin-1/2 and 3/2 baryons. In the pure valence-valence sector,

$$B_{(\text{valence-valence})} = \begin{pmatrix} \Sigma_b^{+1} & \frac{1}{\sqrt{2}}\Sigma_b^0 & \frac{1}{\sqrt{2}}\Xi_b'^{+1/2} \\ \frac{1}{\sqrt{2}}\Sigma_b^0 & \Sigma_b^{-1} & \frac{1}{\sqrt{2}}\Xi_b'^{-1/2} \\ \frac{1}{\sqrt{2}}\Xi_b'^{+1/2} & \frac{1}{\sqrt{2}}\Sigma_b^0 & \Omega_b \end{pmatrix}, \quad (18)$$

and similarly for the  $B_{ij}^{*\mu}$  fields. The  $S_{ij}^\mu$  and  $T_{ij}$  fields have the same property as  $\bar{H}_i^{(\bar{b})}$  under the heavy-quark spin transformation  $S_h$ . For the unbroken light-flavour transformation,

$$\begin{aligned} S_{ij}^\mu(x) &\longrightarrow U_i^k(x) U_j^l(x) S_{kl}^\mu(x), \\ T_{ij}(x) &\longrightarrow U_i^k(x) U_j^l(x) T_{kl}(x), \end{aligned} \quad (19)$$

with the flavour indices satisfying Eq. (14). These  $S_{ij}^\mu$  and  $T_{ij}$  are annihilation field operators and we denote the corresponding creation fields by  $\bar{S}_{ij}^\mu$  and  $\bar{T}_{ij}$ .

The Goldstone mesons couple to the above heavy meson and baryon fields in the HH $\chi$ PT Lagrangian via the non-linear realisation

$$\xi \equiv e^{i\Phi/f} = \sqrt{\Sigma}, \quad (20)$$

which transforms as

$$\xi(x) \longrightarrow U_L \xi(x) U^\dagger(x) = U(x) \xi(x) U_R^\dagger. \quad (21)$$

The  $\xi$  field can be used to construct vector and axial-vector fields

$$\begin{aligned} V^\mu &= \frac{1}{2} (\xi^\dagger \partial^\mu \xi + \xi \partial^\mu \xi^\dagger), \\ A^\mu &= \frac{i}{2} (\xi^\dagger \partial^\mu \xi - \xi \partial^\mu \xi^\dagger). \end{aligned} \quad (22)$$

The vector field can then serve as the gauge field in defining the chiral covariant derivative which acts on the heavy hadrons,

$$\begin{aligned} \mathcal{D}^\mu H_i^{(\bar{b})} &= \partial^\mu H_i^{(\bar{b})} + (V^\mu)_i^j H_j^{(\bar{b})}, \\ \mathcal{D}^\mu T_{ij} &= \partial^\mu T_{ij} + (V^\mu)_i^k T_{kj} + (-1)^{\eta_i(\eta_j+\eta_k)} (V^\mu)_j^k T_{ik}, \\ \mathcal{D}^\mu S_{ij}^\nu &= \partial^\mu S_{ij}^\nu + (V^\mu)_i^k S_{kj}^\nu + (-1)^{\eta_i(\eta_j+\eta_k)} (V^\mu)_j^k S_{ik}^\nu. \end{aligned} \quad (23)$$

The leading-order HH $\chi$ PT Lagrangian is then

$$\begin{aligned} \mathcal{L}_{\text{HH}\chi\text{PT}}^{(\text{LO})} &= -i \text{tr}_D \left[ \bar{H}^{(\bar{b})i} v_\mu \mathcal{D}^\mu H_i^{(\bar{b})} \right] + i (\bar{T} v_\mu \mathcal{D}^\mu T)_f - i (\bar{S}^\nu v_\mu \mathcal{D}^\mu S_\nu)_f + \Delta^{(B)} (\bar{S}^\nu S_\nu)_f \\ &\quad + g_1 \text{tr}_D \left[ \bar{H}_i^{(\bar{b})} \gamma^\mu \gamma_5 H_j^{(\bar{b})} A_\mu^{ij} \right] - i g_2 \epsilon_{\mu\nu\sigma\rho} (\bar{S}^\mu v^\nu A^\sigma S^\rho)_f + \sqrt{2} g_3 \left[ (\bar{T} A^\mu S_\mu)_f + (\bar{S}_\mu A^\mu T)_f \right], \end{aligned} \quad (24)$$

where  $v_\mu$  is the velocity of the heavy hadrons,  $\text{tr}_D[ ]$  means taking the trace in Dirac space, and  $( )_f$  is the implementation of the PQ-theory flavour contraction rules [25]

$$\begin{aligned} (\bar{T} Y T)_f &= \bar{T}^{ji} Y_i^l T_{lj}, \\ (\bar{S}^\mu Y S_\mu)_f &= \bar{S}^{\mu,ji} Y_i^l S_{\mu,lj}, \\ (\bar{T} Y^\mu S_\mu)_f &= \bar{T}^{ji} (Y^\mu)_i^l S_{\mu,lj}. \end{aligned} \quad (25)$$

The parameter  $\Delta^{(B)}$  is the mass difference between the  $S$  and  $T$  fields with the same light flavour indices,

$$\Delta^{(B)} = M_{S_{i,j}} - M_{T_{i,j}}.$$

It is grouped together with the definition of other mass parameters in Eq. (A1) in Appendix A. This mass difference is of  $O(\Lambda_{\text{QCD}})$ , and does not vanish either in the chiral limit or in the heavy-quark limit.

The LO Lagrangian for  $\text{HH}\chi\text{PT}$  contains terms of  $O(p)$  and no light-quark mass dependence. To generate the flavour  $\text{SU}(3)$  breaking effects in heavy-meson and baryon spectrum, which give rise to the mass differences  $\delta_{i,j}^{(M)}$  and  $\delta_{ij,kl}^{(B)}$  in Eq. (A1), one introduces

$$\begin{aligned} \mathcal{L}_{\text{HH}\chi\text{PT}}^{(\chi)} = & \lambda_1 \text{tr}_D \left[ \bar{H}_i^{(\bar{b})} \chi_\xi^{ij} H_j^{(\bar{b})} \right] + \lambda_2 \text{tr}_D \left[ \bar{H}^{(\bar{b})i} H_i^{(\bar{b})} \right] \text{str}(\chi_\xi) \\ & + \lambda_3 (\bar{S}^\mu \chi_\xi S_\mu)_f + \lambda_4 (\bar{S}^\mu S_\mu)_f \text{str}(\chi_\xi) + \lambda_5 (\bar{T} \chi_\xi T)_f + \lambda_6 (\bar{T} T)_f \text{str}(\chi_\xi), \end{aligned} \quad (26)$$

where

$$\chi_\xi = \xi \chi \xi + \xi^\dagger \chi \xi^\dagger. \quad (27)$$

In the computation of the axial-current matrix elements, the flavour breaking effects in Eq. (26) are formally sub-leading compared to those encoded in the pure Goldstone Lagrangian, Eq. (3). Nevertheless, we keep them in our calculation as they can be numerically significant.

In this work, we also include the heavy quark spin symmetry breaking term

$$\frac{\bar{\lambda}_2}{M_B} \text{tr}_D \left[ \bar{H}^{(\bar{b})i} \sigma_{\mu\nu} H_i^{(\bar{b})} \sigma^{\mu\nu} \right], \quad (28)$$

where  $M_B$  is the  $B$  meson mass. This counterterm leads to the mass difference between the  $B^*$  and  $B$  mesons with the same light flavour,

$$\Delta^{(M)} = M_{B_i^*} - M_{B_i},$$

which vanishes in the heavy-quark limit. This mass difference is also grouped together with other mass parameters in Eq. (A1) in Appendix A. In principle, there are also such heavy quark spin breaking terms in the baryon sector, resulting in mass differences between  $B_{ij}$  and  $B_{ij}^*$  baryons in Eq. (17). However, these mass differences are numerically much smaller than  $\Delta^{(M)}$  [26].

### III. AXIAL CURRENT MATRIX ELEMENTS AT THE NEXT-TO-LEADING ORDER

Applying the Noether theorem to the chiral Lagrangian in the previous section, one can derive the leading-order axial currents corresponding to their quark-level counterparts in Eq. (1). For matrix elements involving external states of single heavy hadrons, the relevant LO currents are

$$J_{ij,\mu}^{(N_f)} = g_1 \text{tr}_D \left[ \bar{H}_k^{(\bar{b})} \gamma_\mu \gamma_5 H_l^{(\bar{b})} \left( \tau_{ij,\xi}^{(+)} \right)^{kl} \right] - i g_2 \epsilon_{\mu\nu\rho\sigma} (\bar{S}^\nu v^\sigma \tau_{ij,\xi}^{(+)} S^\rho)_f + \sqrt{2} g_3 \left[ (\bar{S}_\mu \tau_{ij,\xi}^{(+)} T)_f + (\bar{T} \tau_{ij,\xi}^{(+)} S_\mu)_f \right], \quad (29)$$

where the subscript  $ij$  means the current changes the light quark flavours from  $i$  to  $j$ , and

$$\tau_{ij,\xi}^{(+)} = \frac{1}{2} (\xi^\dagger \tau_{ij} \xi + \xi \tau_{ij} \xi^\dagger), \quad (30)$$

with the matrices  $\tau_{ij}$  defined as

$$(\tau_{ij})_{kl} = \delta_{il} \delta_{jk}, \quad (31)$$

where  $k$  and  $l$  run through all the light-quark flavours in PQCD. The superscript  $N_f$  is the number of sea quark flavours and  $N_f = 2, 3$  represent the cases of  $\text{SU}(4|2)$  and  $\text{SU}(6|3)$  respectively. These leading-order axial currents

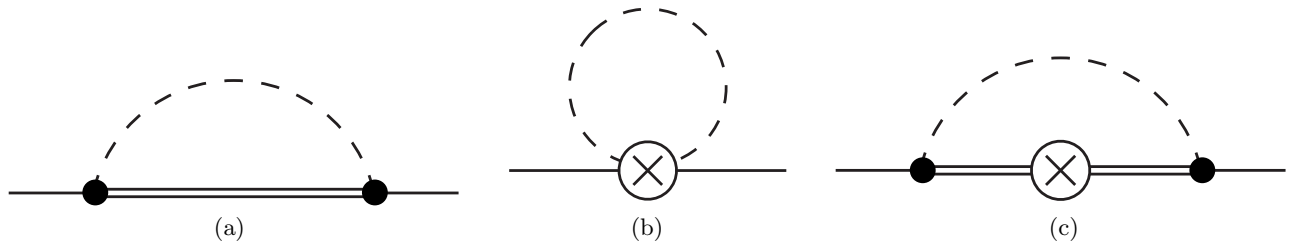


FIG. 1: One-loop diagrams contributing to the matrix elements of axial currents between heavy hadrons. The dashed lines are the Goldstone meson propagators, including the possible “hairpin” structures. The single solid lines denote generically the external heavy hadrons, while the double solid lines are the internal heavy hadrons. They can be  $B$ ,  $B^*$  mesons or  $T_{ij}$ ,  $S_{ij}$  baryons. The circled crosses are the insertions of the LO axial current  $J_{ij,\mu}^{(N_f)}$  given in Eq. (29), while the other vertices are from the strong chiral Lagrangian in Eq. (24). Diagram (a) is the self-energy of the heavy hadron and it leads to the wavefunction renormalisation contribution to the matrix elements. Diagrams (b) and (c) are the “tadpole” and “sunset” types respectively.

generate the LO terms, as well as the NLO contributions via one-loop corrections, in the matrix elements studied in this work<sup>6</sup>.

There is a significant increase in the number of terms in the next-to-leading order axial currents in HH $\chi$ PT, and we postpone the detailed investigation of these NLO currents to Subsection III B below. Here we first write down the generic form of the chiral expansion of the axial-current matrix elements to the NLO,

$$\langle H_j | \mathcal{J}_{ij,\mu} | H_i \rangle_{\text{QCD}} = \langle H_j | J_{ij,\mu}^{(N_f)} | H_i \rangle_{\text{LO}} \times \left[ 1 + \frac{1}{f^2} \left( \mathcal{T}_{ij}^{(N_f)} + \mathcal{W}_{H_i}^{(N_f)} + \mathcal{W}_{H_j}^{(N_f)} + \mathcal{Q}_{H_i \rightarrow H_j}^{(N_f)} \right) + \mathcal{N}_{H_i \rightarrow H_j}^{(N_f)} \right], \quad (32)$$

where the equality symbol means the matching between (PQ)QCD and the chiral effective theory,  $\mu$  is the Lorentz index, and  $\mathcal{J}_{ij,\mu}$  are the quark-level currents given in Eq. (1). The flavour indices are denoted by  $i$  and  $j$  which are *not* summed in the above expression, and  $H_i$  is a heavy hadron state (meson or baryon) containing the light flavour  $i$ . The symbols  $\mathcal{T}_{ij}^{(N_f)}$ ,  $\mathcal{W}_{H_i}^{(N_f)}$  and  $\mathcal{Q}_{H_i \rightarrow H_j}^{(N_f)}$  are results from the tadpole, wavefunction-renormalisation and sunset diagrams at one-loop, as depicted in Fig 1, where single and double solid lines represent generically the external and internal heavy hadrons while the dashed lines are the Goldstone propagators. The circled crosses in Fig 1 are the insertions of the LO axial current  $J_{ij,\mu}^{(N_f)}$  given in Eq. (29). The tadpole contributions  $\mathcal{T}_{ij}^{(N_f)}$  are independent of the external states, since they emerge completely from the flavour structure of the currents.

In Eq. (32), we have written the NLO analytic terms as the LO matrix elements times  $\mathcal{N}_{H_i \rightarrow H_j}^{(N_f)}$ . In Subsection III B below, we will study these NLO analytic terms, and show that they can be presented in this manner. In this section, we examine the analytic terms (polynomials in the Goldstone masses) in the matrix elements in Eq. (32) for various external states. These are encoded in

$$\langle H_j | J_{ij,\mu}^{(N_f)} | H_i \rangle_{\text{LO}} \text{ and } \mathcal{N}_{H_i \rightarrow H_j}^{(N_f)}.$$

The non-analytic contributions arising from the one-loop diagrams will be discussed in Sections IV and V.

### A. Leading-order matrix elements

Lattice computations are often performed using the baryon interpolating fields in Eq. (13). Therefore we carry out the  $\chi$ PT calculation for the  $T_{ij}$  and  $S_{ij}^\mu$  external states. From our results, it is straightforward to obtain matrix elements

<sup>6</sup> In addition to the terms in Eq. (29), there are other operators in the LO currents arising from the chiral Lagrangian introduced in the previous section. Nevertheless, these terms do not appear in the matrix elements to the order we work at. That is, their contributions to the one-loop corrections vanish.

for physical external baryon states using Eqs. (16) and (18). The leading-order HH $\chi$ PT predictions for the matrix elements studied in this work are

$$\begin{aligned}
\langle B_d^* | J_{ud,\mu}^{(N_f)} | B_u \rangle_{\text{LO}} &= \langle B_s^* | J_{us,\mu}^{(3)} | B_u \rangle_{\text{LO}} = -2 g_1 \varepsilon_\mu^*, \\
\langle S_{dd} | J_{ud,\mu}^{(N_f)} | T_{du} \rangle_{\text{LO}} &= \sqrt{2} \langle S_{sd} | J_{ud,\mu}^{(3)} | T_{su} \rangle_{\text{LO}} = \sqrt{2} \langle S_{ds} | J_{us,\mu}^{(3)} | T_{du} \rangle_{\text{LO}} = \langle S_{ss} | J_{us,\mu}^{(3)} | T_{su} \rangle_{\text{LO}} = -g_3 \bar{U}_\mu \mathcal{U}, \\
\langle S_{dd} | J_{ud,\mu}^{(N_f)} | S_{du} \rangle_{\text{LO}} &= \sqrt{2} \langle S_{sd} | J_{ud,\mu}^{(3)} | S_{su} \rangle_{\text{LO}} = \sqrt{2} \langle S_{ds} | J_{us,\mu}^{(3)} | S_{du} \rangle_{\text{LO}} = \langle S_{ss} | J_{us,\mu}^{(3)} | S_{su} \rangle_{\text{LO}} = -\frac{i}{\sqrt{2}} g_2 v^\sigma \epsilon_{\sigma\mu\nu\rho} \bar{U}^\nu U^\rho,
\end{aligned} \tag{33}$$

where  $\varepsilon^\mu$  is the polarisation vector of the  $B^*$  meson,  $\mathcal{U}$  is the Dirac spinor of the  $T$  baryon, and the  $U^\mu$ 's are the ‘‘superfield spinors’’ of the  $S$  baryons. The basis polarisation vectors and spinors satisfy the spin sums

$$\begin{aligned}
\sum_{s=1}^3 \varepsilon_\mu(v, s) \varepsilon_\nu^*(v, s) &= -g_{\mu\nu} + v_\mu v_\nu, \\
\sum_{s=1}^2 \mathcal{U}(v, s) \bar{\mathcal{U}}(v, s) &= \frac{1 + \not{v}}{2}, \\
\sum_{s=1}^6 U^\mu(v, s) \bar{U}^\nu(v, s) &= -(g^{\mu\nu} - v^\mu v^\nu) \frac{1 + \not{v}}{2}.
\end{aligned} \tag{34}$$

Note that  $U^\mu$  is *not* a Rarita-Schwinger spinor; instead it contains the degrees of freedom of both the spin-1/2 and spin-3/2 components of the superfield. In Eq. (33), the states are normalized as

$$\begin{aligned}
\langle B_i(v, \mathbf{k}) | B_i(v, \mathbf{k}') \rangle &= 2v^0 (2\pi)^3 \delta^3(\mathbf{k} - \mathbf{k}'), \\
\langle B_i^*(v, \mathbf{k}, s) | B_i^*(v, \mathbf{k}', s') \rangle &= 2v^0 (2\pi)^3 \delta_{ss'} \delta^3(\mathbf{k} - \mathbf{k}'), \\
\langle T_{ij}(v, \mathbf{k}, s) | T_{ij}(v, \mathbf{k}', s') \rangle &= v^0 (2\pi)^3 \delta_{ss'} \delta^3(\mathbf{k} - \mathbf{k}'), \\
\langle S_{ij}(v, \mathbf{k}, s) | S_{ij}(v, \mathbf{k}', s') \rangle &= v^0 (2\pi)^3 \delta_{ss'} \delta^3(\mathbf{k} - \mathbf{k}').
\end{aligned} \tag{35}$$

## B. Next-to-leading order analytic terms

In this subsection, we investigate the NLO counterterms in the axial currents. Their matrix elements between single heavy hadron states are written as

$$\langle H_j | J_{ij,\mu}^{(N_f)} | H_i \rangle_{\text{LO}} \times \mathcal{N}_{H_i \rightarrow H_j}^{(N_f)},$$

in Eq. (32). These NLO counterterms play a significant role in the chiral expansion, since they have to be included to renormalise the one-loop contributions from the LO axial currents to matrix elements.

First we notice that the chiral Lagrangian in Eq. (26) does not contain any space-time derivative, therefore it does not lead to new terms in the axial currents upon applying the Noether theorem. To obtain the NLO axial currents, we introduce additional operators in the chiral Lagrangian,

$$\begin{aligned}
\mathcal{L}_{\text{HH}\chi\text{PT}}^{(\text{NLO, axial})} &= \kappa_1^{(H)} \text{tr}_D \left[ \bar{H}_i^{(\bar{b})} \gamma^\mu \gamma_5 H_j^{(\bar{b})} (A_\mu)^i{}_k \chi_\xi^{kj} \right] + \kappa_2^{(H)} \text{tr}_D \left[ \bar{H}_i^{(\bar{b})} \gamma^\mu \gamma_5 H_j^{(\bar{b})} \chi_\xi^{ik} (A_\mu)_k^j \right] \\
&+ \kappa_3^{(H)} \text{tr}_D \left[ \bar{H}_i^{(\bar{b})} \gamma^\mu \gamma_5 H_j^{(\bar{b})} (A_\mu)^{ij} \right] \text{str}(\chi_\xi) + \kappa_4^{(H)} \text{tr}_D \left[ \bar{H}_i^{(\bar{b})} \gamma^\mu \gamma_5 H_i^{(\bar{b})} (A_\mu)_{kl} \chi_\xi^{lk} \right] \\
&+ \kappa_1^{(S)} \epsilon_{\mu\nu\sigma\rho} (\bar{S}^\mu v^\nu A^\sigma \chi_\xi S^\rho)_f + \kappa_2^{(S)} \epsilon_{\mu\nu\sigma\rho} (\bar{S}^\mu v^\nu \chi_\xi A^\sigma S^\rho)_f \\
&+ \kappa_3^{(S)} \epsilon_{\mu\nu\sigma\rho} (\bar{S}^\mu v^\nu A^\sigma S^\rho)_f \text{str}(\chi_\xi) + \kappa_4^{(S)} \epsilon_{\mu\nu\sigma\rho} (\bar{S}^\mu v^\nu S^\rho)_f \text{str}(A^\sigma \chi_\xi) \\
&+ \kappa_1^{(T)} \left[ (\bar{T} A^\mu \chi_\xi S_\mu)_f + (\bar{S}_\mu A^\mu \chi_\xi T)_f \right] + \kappa_2^{(T)} \left[ (\bar{T} \chi_\xi A^\mu S_\mu)_f + (\bar{S}_\mu \chi_\xi A^\mu T)_f \right] \\
&+ \kappa_3^{(T)} \left[ (\bar{T} A^\mu S_\mu)_f + (\bar{S}_\mu A^\mu T)_f \right] \text{str}(\chi_\xi),
\end{aligned} \tag{36}$$

where  $\chi_\xi$  is defined in Eq. (27). The mesonic sector of the above Lagrangian was already introduced in Refs. [23, 27]. Upon applying the Noether theorem to Eq. (36), one obtains the currents which lead to the NLO analytic terms  $\mathcal{N}_{H_i \rightarrow H_j}^{(N_f)}$  in Eq. (32),

$$\begin{aligned}
J_{ij,\mu}^{(\text{NLO, analytic})} &= \kappa_1^{(H)} \text{tr}_D \left[ \bar{H}_k^{(\bar{b})} \gamma_\mu \gamma_5 H_l^{(\bar{b})} \left( \tau_{ij,\xi}^{(+)} \chi_\xi \right)^{kl} \right] + \kappa_2^{(H)} \text{tr}_D \left[ \bar{H}_k^{(\bar{b})} \gamma_\mu \gamma_5 H_l^{(\bar{b})} \left( \chi_\xi \tau_{ij,\xi}^{(+)} \right)^{kl} \right] \\
&+ \kappa_3^{(H)} \text{tr}_D \left[ \bar{H}_k^{(\bar{b})} \gamma_\mu \gamma_5 H_l^{(\bar{b})} \left( \tau_{ij,\xi}^{(+)} \right)^{kl} \right] \text{str}(\chi_\xi) + \kappa_4^{(H)} \text{tr}_D \left[ \bar{H}_k^{(\bar{b})} \gamma_\mu \gamma_5 H_k^{(\bar{b})} \left( \tau_{ij,\xi}^{(+)} \chi_\xi \right)^{ll} \right] \\
&+ \kappa_1^{(S)} \epsilon_{\mu\nu\sigma\rho} (\bar{S}^\nu v^\sigma \tau_{ij,\xi}^{(+)} \chi_\xi S^\rho)_f + \kappa_2^{(S)} \epsilon_{\mu\nu\sigma\rho} (\bar{S}^\nu v^\sigma \chi_\xi \tau_{ij,\xi}^{(+)} S^\rho)_f \\
&+ \kappa_3^{(S)} \epsilon_{\mu\nu\sigma\rho} (\bar{S}^\nu v^\sigma \tau_{ij,\xi}^{(+)} S^\rho)_f \text{str}(\chi_\xi) + \kappa_4^{(S)} \epsilon_{\mu\nu\sigma\rho} (\bar{S}^\nu v^\sigma S^\rho)_f \text{str} \left( \tau_{ij,\xi}^{(+)} \chi_\xi \right) \\
&+ \kappa_1^{(T)} \left[ (\bar{T} \tau_{ij,\xi}^{(+)} \chi_\xi S_\mu)_f + (\bar{S}_\mu \tau_{ij,\xi}^{(+)} \chi_\xi T)_f \right] + \kappa_2^{(T)} \left[ (\bar{T} \chi_\xi \tau_{ij,\xi}^{(+)} S_\mu)_f + (\bar{S}_\mu \chi_\xi \tau_{ij,\xi}^{(+)} T)_f \right] \\
&+ \kappa_3^{(T)} \left[ (\bar{T} \tau_{ij,\xi}^{(+)} S_\mu)_f + (\bar{S}_\mu \tau_{ij,\xi}^{(+)} T)_f \right] \text{str}(\chi_\xi), \tag{37}
\end{aligned}$$

where  $\tau_{ij,\xi}^{(+)}$  is defined in Eq. (30). Although it is not explicitly shown in the above equation, these NLO currents depend on  $N_f$ .

Comparing the currents  $J_{ij,\mu}^{(\text{NLO, analytic})}$  to their leading-order counterparts,  $J_{ij,\mu}^{(N_f)}$  in Eq. (29), one observes that they share the similar feature in the combination of the heavy-hadron fields with the flavour matrices  $\tau_{ij,\xi}^{(+)}$ . The complication in  $J_{ij,\mu}^{(\text{NLO, analytic})}$  results completely from the insertion of  $\chi_\xi$ , which contains one power of the quark-mass matrix. This shows that one can write the NLO matrix elements as

$$\langle H_j | J_{ij,\mu}^{(\text{NLO, analytic})} | H_i \rangle_{\text{NLO}} = \langle H_j | J_{ij,\mu}^{(N_f)} | H_i \rangle_{\text{LO}} \times \mathcal{N}_{H_i \rightarrow H_j}^{(N_f)},$$

and

$$\mathcal{N}_{H_i \rightarrow H_j}^{(N_f)} \sim O(m_q) \sim O(M_{\text{Goldstone}}^2),$$

where  $m_q$  is the light-quark mass.

#### IV. ONE-LOOP CONTRIBUTIONS IN SU(2) HH $\chi$ PT

We now turn to the discussion of the one-loop results for the axial-current matrix elements. In this section, we first present a simple case, namely SU(2)  $\chi$ PT in the infinite-volume limit, and use it to illustrate the main features of these one-loop contributions. Details of the SU(4|2) and SU(6|3) PQ $\chi$ PT results are addressed in the next section.

We start by reducing the leading-order matrix elements in Eq. (33) to a simpler form. Notice that all these matrix elements are proportional to the axial couplings,  $g_{1,2,3}$ . Therefore, from the generic form of the chiral expansion for the axial-current matrix elements given in Eq. (32), we can define the ‘‘effective’’ axial couplings

$$\begin{aligned}
(g_1)_{\text{eff}} &= g_1 \times \left[ 1 + \frac{1}{f^2} \left( \mathcal{T}_{ud}^{(2)} + \mathcal{W}_{B_u}^{(2)} + \mathcal{W}_{B_d^*}^{(2)} + \mathcal{Q}_{B_u \rightarrow B_d^*}^{(2)} \right) + \mathcal{N}_{B_u \rightarrow B_d^*}^{(2)} \right], \\
(g_2)_{\text{eff}} &= g_2 \times \left[ 1 + \frac{1}{f^2} \left( \mathcal{T}_{ud}^{(2)} + \mathcal{W}_{T_{du}}^{(2)} + \mathcal{W}_{S_{dd}}^{(2)} + \mathcal{Q}_{T_{du} \rightarrow S_{dd}}^{(2)} \right) + \mathcal{N}_{T_{du} \rightarrow S_{dd}}^{(2)} \right], \\
(g_3)_{\text{eff}} &= g_3 \times \left[ 1 + \frac{1}{f^2} \left( \mathcal{T}_{ud}^{(2)} + \mathcal{W}_{S_{du}}^{(2)} + \mathcal{W}_{S_{dd}}^{(2)} + \mathcal{Q}_{S_{du} \rightarrow S_{dd}}^{(2)} \right) + \mathcal{N}_{S_{du} \rightarrow S_{dd}}^{(2)} \right], \tag{38}
\end{aligned}$$

with the wavefunction renormalisation ( $\mathcal{W}$ ), tadpole ( $\mathcal{T}$ ) and sunset ( $\mathcal{Q}$ ) diagram contributions from Fig. 1 (a), (b) and (c).

The result for the tadpole diagram is particularly simple. In the infinite-volume limit, it is

$$\mathcal{T}_{ud}^{(2)} \xrightarrow{\text{infinite-}V} -2I(M_\pi) = -\frac{2}{16\pi^2} M_\pi^2 \log\left(\frac{M_\pi^2}{\mu^2}\right),$$

following the definition of the function  $I(m)$  in Eq. (B4) in Appendix B. Here  $M_\pi$  is the pion mass, and  $\mu$  is the renormalisation scale. The dependence on  $\mu$  is cancelled by the NLO counterterm contributions  $\mathcal{N}^{(2)}$  in the above expression for the effective axial couplings.

In this SU(2) full QCD case, the infinite-volume limit of the wavefunction renormalisation and sunset diagrams can be written in two functions

$$\begin{aligned} H(m, \Delta) &= \frac{\partial F(m, \Delta)}{\partial \Delta}, \\ K(m, \Delta_1, \Delta_2) &= \frac{F(m, \Delta_1) - F(m, \Delta_2)}{\Delta_1 - \Delta_2}, \end{aligned} \quad (39)$$

with the function  $F$  defined in Eq. (B4). The scale  $\Delta$  in these functions results from the mass difference between the external and the internal heavy hadrons. In the heavy quark and the isospin limits, we have

$$M_{B_d^*} - M_{B_u} = M_{S_{dd}} - M_{S_{du}} = 0.$$

Therefore the only relevant heavy-hadron mass difference in these limits is

$$\Delta^{(B)} = M_{S_{du}} - M_{T_{du}} = M_{S_{dd}} - M_{T_{du}} \sim 200 \text{ MeV},$$

and the effective couplings in Eq. (38) are

$$\begin{aligned} (g_1)_{\text{eff}} &= g_1 \left[ 1 - \frac{2}{f^2} I(M_\pi) + \frac{4g_1^2}{f^2} H(M_\pi, 0) + \text{analytic terms} \right], \\ (g_2)_{\text{eff}} &= g_2 \left[ 1 - \frac{2}{f^2} I(M_\pi) + \frac{3g_2^2}{2f^2} H(M_\pi, 0) + \frac{g_3^2}{f^2} \left( H(M_\pi, -\Delta^{(B)}) - 2K(M_\pi, -\Delta^{(B)}, 0) \right) + \text{analytic terms} \right], \\ (g_3)_{\text{eff}} &= g_3 \left[ 1 - \frac{2}{f^2} I(M_\pi) + \frac{g_2^2}{f^2} \left( -2H(M_\pi, \Delta^{(B)}) + H(M_\pi, 0) \right) \right. \\ &\quad \left. + \frac{g_3^2}{2f^2} \left( H(M_\pi, -\Delta^{(B)}) + 9H(M_\pi, \Delta^{(B)}) - 2K(M_\pi, \Delta^{(B)}, 0) \right) + \text{analytic terms} \right], \end{aligned} \quad (40)$$

with the analytic terms resulting from  $\mathcal{N}^{(2)}$  in Eq. (38). Here we stress that the tadpole diagram is the dominant one-loop contribution to the chiral expansion of  $(g_1)_{\text{eff}}$ . This is because the typical value of the coupling,  $g_1^2 \sim 0.25$ , is small, leading to the suppression of other diagrams in the above equation<sup>7</sup>. A numerical comparison of the individual contributions from different types of Feynman diagrams will be given in Sec. IV B.

Before proceeding with further discussion of the formulae in Eq. (40), we notice that the function  $H(m, \Delta)$  can be related to  $I(m)$  when  $\Delta = 0$ ,

$$H(m, 0) = -I(m) = -\frac{m^2}{16\pi^2} \log\left(\frac{m^2}{\mu^2}\right). \quad (41)$$

This leads to the simplification of the chiral expansion of  $(g_1)_{\text{eff}}$ ,

$$(g_1)_{\text{eff}} = g_1 \left[ 1 - \frac{2}{(4\pi f)^2} M_\pi^2 \log\left(\frac{M_\pi^2}{\mu^2}\right) - \frac{4g_1^2}{(4\pi f)^2} M_\pi^2 \log\left(\frac{M_\pi^2}{\mu^2}\right) + c(\mu) M_\pi^2 \right]. \quad (42)$$

<sup>7</sup> Since  $g_{2,3} \sim O(1)$ , this suppression is not present in the chiral expansion of  $(g_{2,3})_{\text{eff}}$ .

The renormalisation-scale dependence from the loop diagrams is cancelled by the coefficient,  $c(\mu)$ , of the analytic term which also encodes the contributions from the NLO Lagrangian.

In the following two subsections, we first address an issue related to the chiral limit of the formulae presented above, and then present an estimation for the numerical size of the one-loop corrections.

### A. Wavefunction renormalisation and sunset diagrams in the chiral limit

As pointed out in Eqs. (39) and (40), the infinite-volume one-loop contributions from the wavefunction renormalisation and sunset diagrams can be written in terms of the functions  $H$  and  $K$ , which are obtained by taking derivatives of the function defined in Eq. (B4),

$$F(m, \Delta) = \frac{-1}{16\pi^2} \left[ \left( m^2 - \frac{2\Delta^2}{3} \right) \Delta \log \left( \frac{m^2}{\mu^2} \right) + \left( \frac{10\Delta^2}{9} - \frac{4m^2}{3} \right) \Delta + \frac{2(\Delta^2 - m^2)}{3} m R \left( \frac{\Delta}{m} \right) \right], \text{ where}$$

$$R(x) \equiv \sqrt{x^2 - 1} \left[ \log \left( x - \sqrt{x^2 - 1 + i\epsilon} \right) - \log \left( x + \sqrt{x^2 - 1 + i\epsilon} \right) \right].$$

This function is obtained by regularising the loop integrals with the subtraction scheme defined in Eq. (B1) in Appendix B. Implementing this scheme is a common practice in  $\chi$ PT calculations [28]. It leads to the result that  $F(m, \Delta)$  does not vanish in the limit  $m \rightarrow 0$  unless  $\Delta = 0$ . Such behaviour does not cause any conceptual problem in the effective theory, since the axial couplings,  $g_{1,2,3}$ , can undergo finite renormalisation depending on the subtraction scheme used to regulate one-loop integrals. Various subtraction schemes always lead to the same physical quantities, such as the hadronic masses and axial transition amplitudes, which are scheme-independent. On the other hand, it would be desirable and natural to choose a scheme in which the one-loop contributions decouple in the chiral limit. As pointed out in Refs. [29, 30], it is possible to find a scheme such that the real part of  $F$  vanishes in the chiral limit. It is implemented by simply rewriting  $F$  as

$$F^{(\text{sub})}(m, \Delta) = \frac{-1}{16\pi^2} \left[ m^2 \Delta \log \left( \frac{m^2}{\mu^2} \right) - \frac{2\Delta^3}{3} \log \left( \frac{m^2}{4\Delta^2} \right) - \frac{4m^2\Delta}{3} + \frac{2(\Delta^2 - m^2)}{3} m R \left( \frac{\Delta}{m} \right) \right], \quad (43)$$

and appropriately modifying the counterterms to absorb the difference (a finite polynomial in  $\Delta$ ). It is straightforward to demonstrate that when  $\Delta + m > 0$ , in which case the external heavy hadrons are stable particles, this function is real and

$$\lim_{m \rightarrow 0} F^{(\text{sub})}(m, \Delta) = 0. \quad (44)$$

In the case  $\Delta + m < 0$  which corresponds to the situation that the external heavy hadron becomes unstable, the functions  $F$  and  $F^{(\text{sub})}$  are complex. Although the real part of  $F^{(\text{sub})}$  vanishes in the chiral limit, the imaginary part remains non-zero. This occurs when

$$M_\pi < |M_{T_{ij}} - M_{S_{ij}^\mu}| = \Delta^{(B)} \sim 200 \text{ MeV}. \quad (45)$$

Below this threshold, one cannot define matrix elements containing external  $S_{ij}^\mu$  hadrons. In principle, more complicated matrix elements can be used to determine the couplings  $g_2$  and  $g_3$  for the pion masses in the regime of Eq. (45), but this is beyond the scope of this work. See Refs. [31, 32] for related discussions. Here we stress that one can perform lattice calculations in the regime where the pion mass is larger than  $\Delta^{(B)}$  but small compared to the chiral symmetry breaking scale, such that the external hadrons are all stable and the chiral expansion is still valid. These calculations enable the extraction the axial couplings,  $g_{1,2,3}$ , which can then be used to perform chiral extrapolations and make predictions for other quantities.

### B. Evaluation of individual contributions

In this subsection, we use the simple infinite volume, SU(2) case to explore the typical size of the one-loop contributions. This can be best summarised by the plots in Fig. 2. In these plots, the pion mass dependence of the loop contributions

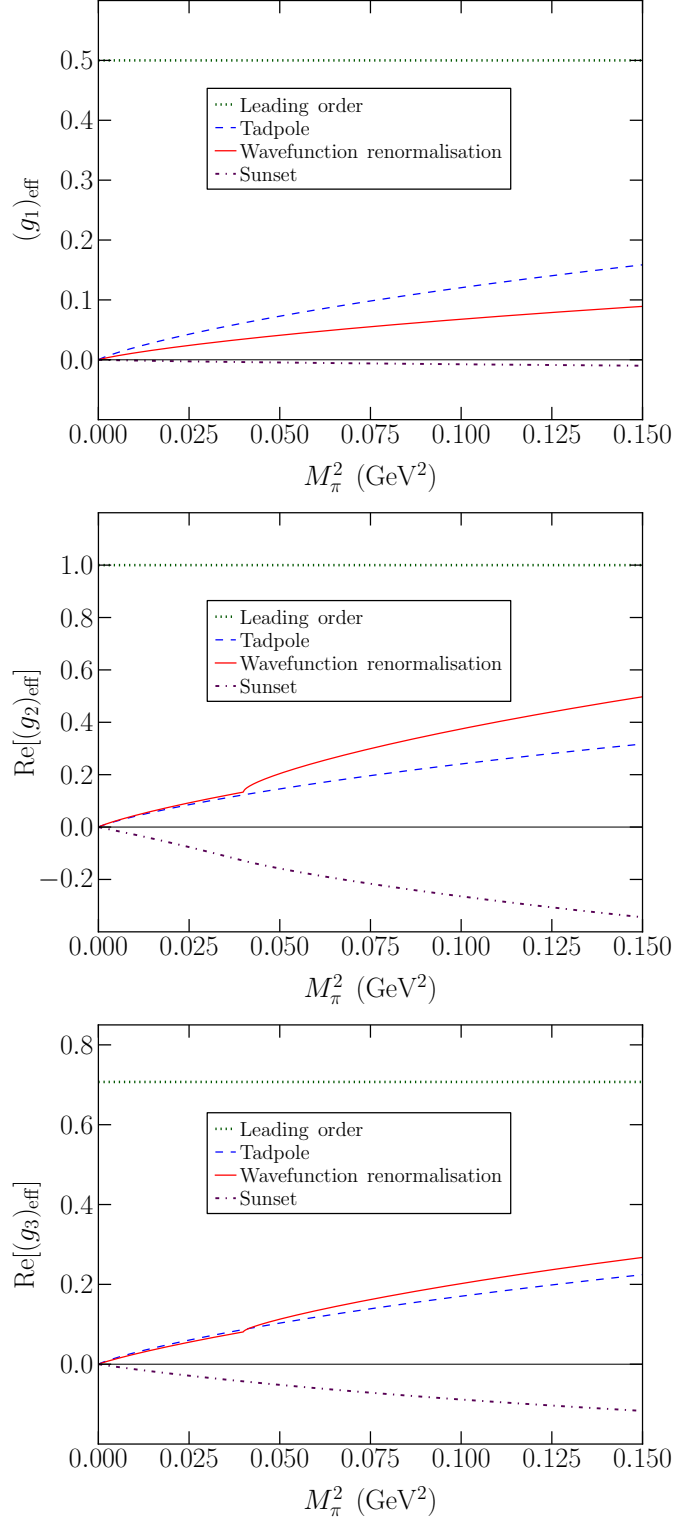


FIG. 2: Comparison of the individual infinite-volume one-loop contributions to the pion mass dependence of the (real part of the) various effective couplings,  $(g_{1,2,3})_{\text{eff}}$  evaluated using the values of the LECs given in the text. The kinks in the wavefunction renormalisation and sunset contributions to the baryonic couplings arise from the  $S \rightarrow T\pi$  threshold at  $M_\pi = \Delta^{(B)}$ . Below this threshold, the curves lose their physical interpretation. The subtraction scheme is that presented in Eq. (43).

to three effective axial couplings [their real part in the case of  $(g_{2,3})_{\text{eff}}$ ] is shown for exemplary values of the various low energy constants. These results are obtained using the subtraction scheme defined in Eq. (43) in Sec. IV A. The leading order contribution is also shown. We take  $g_1 = 0.5$ , a value consistent with recent determinations [12–17] and then use the quark model expectations for the other couplings,  $g_2 = 2g_1$  and  $g_3 = \sqrt{2}g_1$  (in our normalisation) [3]<sup>8</sup> which are far less constrained. We work in the heavy-quark limit so that  $\Delta^{(M)} = 0$ , and we have set the  $S - T$  mass differences to  $\Delta^{(B)} = 200$  MeV, consistent with experiment [26]. The renormalization scale used here is  $\mu = 4\pi f$ .

It is clear from these figures that the tadpole contributions provide an important part of the chiral non-analytic behaviour of the axial couplings. Furthermore, in the range of pion masses considered here,  $M_\pi \lesssim 400$  MeV, the NLO contributions from loops are numerically small corrections to the leading-order results.<sup>9</sup> This indicates that in this range the  $SU(2)$  chiral expansion of the axial-current matrix elements is well-behaved. Variations of the low-energy constants,  $g_1, g_2, g_3, \Delta^{(B)}$ , and the renormalisation scale,  $\mu$ , within reasonable ranges do not substantially alter the behaviour shown in Fig. 2.

## V. ONE-LOOP CONTRIBUTIONS IN $SU(4|2)$ AND $SU(6|3)$ $\text{HH}\chi\text{PT}$

In this section, we study the one-loop contributions in Eq. (32) in  $SU(4|2)$  and  $SU(6|3)$  partially quenched  $\text{HH}\chi\text{PT}$  in finite volume. These results are complicated because we keep the  $SU(3)$  light-flavour breaking effects from Eq. (26) in our calculation. Here we investigate the structure of the one-loop computation via analysing the quark flavour flow picture [34]. The details of the results are given in Appendices C and D.

### A. The tadpole diagrams

First we present the contributions from the tadpole diagrams. These take the simple form,

$$\begin{aligned}\mathcal{T}_{ud}^{(2)} &= -2\mathcal{I}(M_{u,u'}), \\ \mathcal{T}_{ud}^{(3)} &= -2\mathcal{I}(M_{u,u'}) - \mathcal{I}(M_{u,s'}), \\ \mathcal{T}_{us}^{(3)} &= -\mathcal{I}(M_{u,u'}) - \frac{1}{2}\mathcal{I}(M_{u,s'}) - \mathcal{I}(M_{s,u'}) - \frac{1}{2}\mathcal{I}(M_{s,s'}) + \frac{1}{6}\tilde{\mathcal{I}}_3(M_{u,u}) - \frac{1}{3}\tilde{\mathcal{I}}_3(M_{u,s}) + \frac{1}{6}\tilde{\mathcal{I}}_3(M_{s,s}),\end{aligned}\quad (46)$$

where the functions  $\mathcal{I}$  and  $\tilde{\mathcal{I}}_3$  are defined in (B3) and (B13), respectively. The tadpole diagram results are completely determined by the structure of the axial currents.

### B. The self-energy diagrams

In this subsection, we present the heavy hadron wavefunction renormalisation, resulting from the self-energy diagrams. These are more complicated than the tadpole-diagram results in our calculation, since we keep track of the flavour  $SU(3)$  breaking effects from both the Goldstone masses [Eq. (3)] and the heavy-meson and baryon spectrum [Eq. (26)]. It is helpful to analyse the quark flavour flow diagrams [34] to understand the structure of the results. To investigate this structure, we first assign a “direction” to each flavour flow line:

- The flow following the direction of a line means a quark with that flavour, while the flow against the direction means its anti-quark.

<sup>8</sup> These values are also consistent with preliminary lattice QCD results [33].

<sup>9</sup> The imaginary parts of  $(g_{2,3})_{\text{eff}}$  that arise for  $M_\pi < \Delta^{(B)}$  are also small,  $|\text{Im}(g_{2,3})_{\text{eff}}| < 0.05$ .



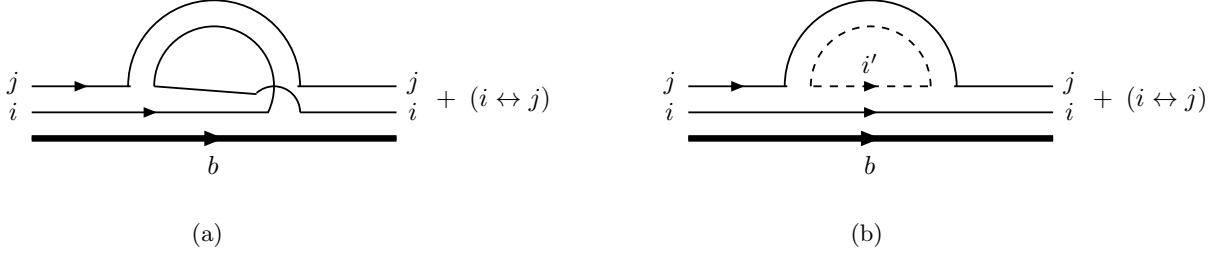


FIG. 4: Quark flavour flow structure for the baryon self-energy diagrams without the “hairpin” structure. The thick line represents the  $b$  quark, and the thin lines are the valence light quarks, while the dashed line is the sea light quark. Diagram (a) is the “crossing” type which does not involve sea quark contributions. The explicitly-shown diagrams give rise to the terms multiplied by  $w$  and  $w'$  in Eq. (48) when the internal baryons are  $S_{ai}$  and  $T_{ai}$  respectively [ $a = i$  in diagram (a) and  $a = i'$  in diagram (b)]. Interchanging the flavour indices  $i$  and  $j$  leads to the corresponding  $u$  and  $u'$  terms in the same equation.

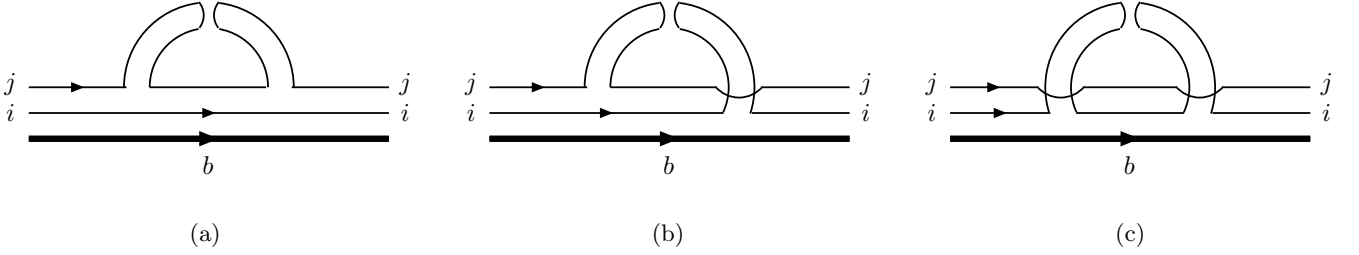


FIG. 5: Quark flavour flow structure for the baryon self-energy diagrams involving the “hairpin” structure. The thick line represents the  $b$  quark, and the thin lines are the valence light quarks. Diagram (a) contributes to the  $\tilde{w}$  (internal  $S_{ij}$  baryon) and  $\tilde{w}'$  (internal  $T_{ij}$  baryon) terms in Eq. (48), while Diagrams (b) and (c) result in the  $\tilde{u}$  (internal  $S_{ij}$  baryon) and  $\tilde{u}'$  (internal  $T_{ij}$  baryon) terms in the same equation.

The flavour flow structure for the baryon self-energy diagrams can be summarised in Figs. 4 and 5. For the diagrams explicitly shown in Fig. 4 (a) and (b), the Goldstone mesons are composed of  $(j, \text{anti-}i)$  and  $(j, \text{anti-}i')$  respectively. Therefore, they are accompanied by the  $w$ -type coefficients ( $w$  for the internal  $S$  baryon and  $w'$  for the internal  $T$  baryon). Terms with the  $u$ -type coefficients are obtained by exchanging the flavours  $i$  and  $j$ , as also indicated in this figure. Notice that the “non-hairpin” valence-valence Goldstone contributions appear via the “crossing” configuration in Fig 4 (a). The “hairpin” structure of the baryon self-energy diagrams is presented in Fig. 5. From the above rules, it is clear that the diagram in Fig. 5 (a) leads to a  $\tilde{w}$ -type term, while those in Fig. 5 (b) and (c) are multiplied by  $\tilde{u}$ -type coefficients.

Following the above discussion, we obtain the results for the baryon wavefunction renormalisation,

$$\begin{aligned}
\mathcal{W}_{T_{ij}}^{(N_f)} &= g_3^2 \sum_a \left[ w_{T_{ij},a}^{(N_f)} \mathcal{H}(M_{j,a}, \Delta^{(B)} + \delta_{ai,ij}^{(B)}) + \tilde{w}_{T_{ij},a}^{(N_f)} \tilde{\mathcal{H}}_{N_f}(M_{j,a}, \Delta^{(B)}) \right. \\
&\quad \left. + u_{T_{ij},a}^{(N_f)} \mathcal{H}(M_{i,a}, \Delta^{(B)} + \delta_{aj,ij}^{(B)}) + \tilde{u}_{T_{ij},a}^{(N_f)} \tilde{\mathcal{H}}_{N_f}(M_{i,a}, \Delta^{(B)}) \right], \\
\mathcal{W}_{S_{ij}}^{(N_f)} &= g_2^2 \sum_a \left[ w_{S_{ij},a}^{(N_f)} \mathcal{H}(M_{j,a}, \delta_{ai,ij}^{(B)}) + \tilde{w}_{S_{ij},a}^{(N_f)} \tilde{\mathcal{H}}_{N_f}(M_{j,a}, 0) \right. \\
&\quad \left. + u_{S_{ij},a}^{(N_f)} \mathcal{H}(M_{i,a}, \delta_{aj,ij}^{(B)}) + \tilde{u}_{S_{ij},a}^{(N_f)} \tilde{\mathcal{H}}_{N_f}(M_{i,a}, 0) \right] \\
&\quad + g_3^2 \sum_a \left[ w'_{S_{ij},a}^{(N_f)} \mathcal{H}(M_{j,a}, -\Delta^{(B)} + \delta_{ai,ij}^{(B)}) + \tilde{w}'_{S_{ij},a}^{(N_f)} \tilde{\mathcal{H}}_{N_f}(M_{j,a}, -\Delta^{(B)}) \right. \\
&\quad \left. + u'_{S_{ij},a}^{(N_f)} \mathcal{H}(M_{i,a}, -\Delta^{(B)} + \delta_{aj,ij}^{(B)}) + \tilde{u}'_{S_{ij},a}^{(N_f)} \tilde{\mathcal{H}}_{N_f}(M_{i,a}, -\Delta^{(B)}) \right], \tag{48}
\end{aligned}$$

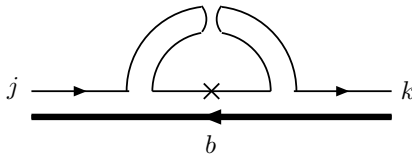


FIG. 6: Quark flavour flow structure for the meson sunset diagrams with external  $B_j$  and  $B_k^*$  states. The thick line represents the anti- $b$  quark, and the thin line is the valence light quark. The cross is the current  $J_{jk}$ . This diagram results in the  $\tilde{y}$  (internal  $B_j^*$  and  $B_k^*$ ) and  $\tilde{y}'$  (internal  $B_j^*$  and  $B_k$ ) terms in Eq. (49). This is the only possible quark flavour flow configuration for the meson sunset diagrams.

where the summations are over the flavours  $u$  and  $u'$  in the SU(4|2) theory, and are over the flavours  $u, s, u'$  and  $s'$  in the SU(6|3) theory. The relevant coefficients,  $w, u \dots$  are presented in Tables II and III in Appendix C. The mass parameters  $M_{a,b}$ ,  $\Delta^{(B)}$  and  $\delta_{ab,cd}^{(B)}$  are defined in Eq. (A1) in Appendix A. These results agree with those in the literature [35]<sup>10</sup>.

### C. The sunset diagrams

In this subsection, we discuss the structure of the sunset diagrams. The Lorentz indices carried by the hadronic states are completely absorbed into the tree-level contribution in Eq. (32), therefore they are omitted in the notation below. In order to organise the results, we follow the same convention in assigning the “flow direction” to a quark line and the “tilded” coefficients to the terms involving the “hairpin” structure, as that in the self-energy diagrams.

First we study the sunset diagram for the axial-current matrix element between the  $B_j$  and  $B_k^*$  mesons. Because of the flavour-changing structure of the currents that we consider in this work, it is straightforward to demonstrate that in this case the Goldstone meson must involve the “hairpin” contribution. This is depicted in Fig. 6. Furthermore, the internal heavy meson with the light flavour  $j$  must be a  $B_j^*$  since there is no  $B$ – $B$ –Goldstone coupling in the Lagrangian or the current. On the other hand, the internal heavy meson involving the light flavour  $k$  can be either  $B_k$  or  $B_k^*$ . These two cases are distinguished by the “primed” and the “unprimed” coefficients in the results. We then obtain the sunset-diagram contribution to this matrix element as

$$\mathcal{Q}_{B_j \rightarrow B_k^*}^{(N_f)} = g_1^2 \left[ \tilde{y}_{B_j, B_k^*}^{(N_f)} \tilde{\mathcal{K}}_{N_f}(M_{j,k}, \Delta^{(M)}, \Delta^{(M)} + \delta_{k,j}^{(M)}) + \tilde{y}'_{B_j, B_k^*} \tilde{\mathcal{K}}_{N_f}(M_{j,k}, \Delta^{(M)}, \delta_{k,j}^{(M)}) \right], \quad (49)$$

where  $\mathcal{K}$  and  $\tilde{\mathcal{K}}_{N_f}$  are the sums (integrals) involved in the loops, and are defined in Eqs. (B9), (B11), (B12) and (B13) in Appendix B. The mass parameters  $M_{j,k}$ ,  $\Delta^{(M)}$  and  $\delta_{k,j}^{(M)}$  are defined in Eq. (A1) in Appendix A. The coefficients  $\tilde{y}$  and  $\tilde{y}'$  are presented in Table VII in Appendix D.

Next, we investigate the sunset diagrams for the following axial-current transitions involving baryons,

$$\begin{aligned} T_{ij} &\longrightarrow S_{ik}^\mu \\ S_{ij}^\mu &\longrightarrow S_{ik}^\nu, \end{aligned} \quad (50)$$

where the spectator quark carries the flavour index  $i$ . The quark flavour flow configurations are shown in Figs. 7, 8 and 9. Again, we use the “tilded” coefficients to denote terms in which the “hairpin” structure appears. Because of parity, there are no axial couplings amongst even number of Goldstone mesons, therefore the flavour indices  $j$  and  $k$  must appear in the internal baryons. These internal baryons can be  $T$  or  $S$  type. Denoting the other flavour index in the loop by  $a$ , we adopt the following convention to distinguish various possibilities for the internal  $S$  and  $T$  contributions:

<sup>10</sup> The SU(3) breaking effects arising from Eq. (26) are not included in the results in Ref. [35]. We have also checked these wavefunction renormalisation diagrams against the full-QCD, SU(3)-limit results at  $\Delta^{(B)} = 0$  in Ref. [5], and found agreement.

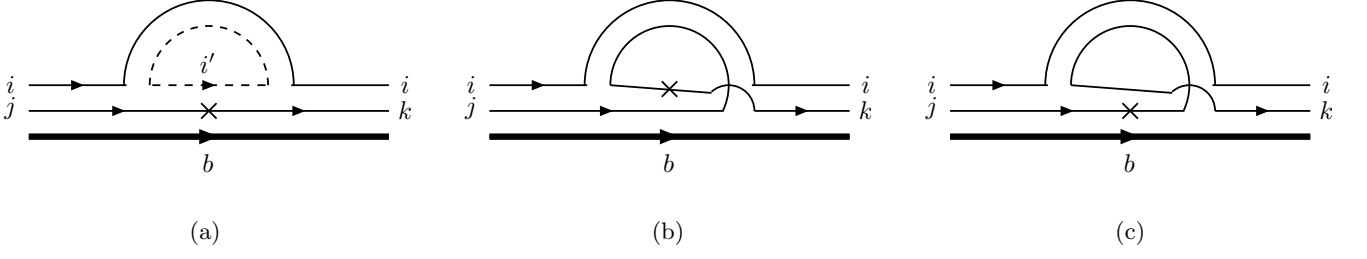


FIG. 7: Quark flavour flow structure for the baryon sunset diagrams without the “hairpin” structure. The thick line represents the  $b$  quark, and the thin lines are the valence light quarks, while the dashed line is the sea light quark. The cross is the current  $J_{jk}$ . These diagrams lead to the  $x$  (internal  $S_{aj}$  and  $S_{ak}$  baryons with  $a = i', j, k$  in diagram (a), (b), (c) respectively),  $x'$  (internal  $T_{aj}$  and  $S_{ak}$  baryon ) and  $x''$  (internal  $S_{aj}$  and  $T_{ak}$  baryons) terms in Eq. (51).

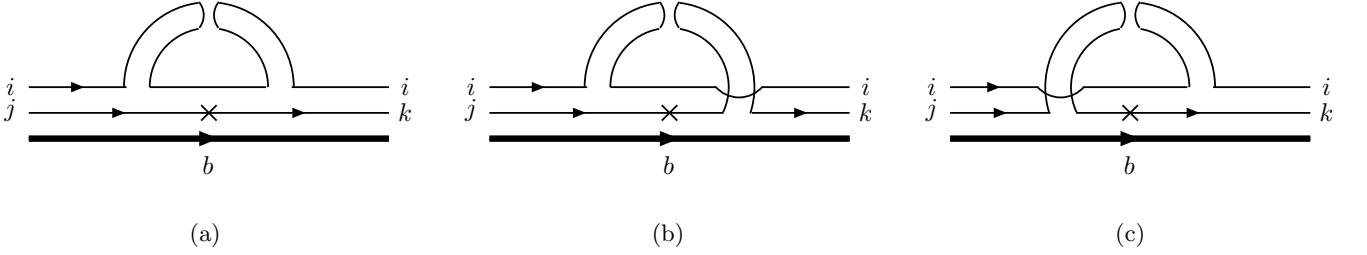


FIG. 8: Quark flavour flow structure for the baryon sunset diagrams with the “hairpin” structure involving the spectator quark (flavour  $i$ ). The thick line represents the  $b$  quark, and the thin lines are the valence light quarks. The cross is the current  $J_{jk}$ . These diagrams lead to the  $\tilde{x}$  (internal  $S_{ij}$  and  $S_{ik}$  baryons),  $\tilde{x}'$  (internal  $T_{ij}$  and  $S_{ik}$  baryon ) and  $\tilde{x}''$  (internal  $S_{ij}$  and  $T_{ik}$  baryons) terms in Eq. (51).

- If the internal baryons are  $S_{aj}$  and  $S_{ak}$ , then the coefficient for the diagram is “unprimed”.
- If the internal baryons are  $T_{aj}$  (left in the loop) and  $S_{ak}$  (right in the loop), then the coefficient for the diagram is “primed”. Such terms are absent in the  $T \rightarrow S$  transition amplitudes.
- If the internal baryons are  $S_{aj}$  (left in the loop) and  $T_{ak}$  (right in the loop), then the coefficient for the diagram is “double-primed”.

To keep track of the flow of the spectator quark  $i$  in these processes, we follow the rules:

- If the spectator quark flavour is present in the Goldstone meson, then the diagram corresponds to a term with  $x$ -type coefficient ( $x, x', x'', \tilde{x}, \tilde{x}'$  or  $\tilde{x}''$ ).
- If the spectator quark flavour is absent in the Goldstone meson, then the diagram corresponds to a term with  $y$ -type coefficient.

In Fig. 7, we show the quark flavour flow diagrams containing no “hairpin” structure. In such flow configurations, the spectator quark flavour always appears in the Goldstone meson. Therefore they will only be accompanied by the  $x$ -type coefficients. Notice that the valence-valence Goldstone mesons also appear in these diagrams via the “crossing” configurations in Figs. 7 (b) and (c). The “hairpin” contributions to the quark flavour flow configurations for the processes in Eq. (50) are shown in Figs. 8 and 9. These two figures are distinguished by the presence/absence of the spectator quark flavour in the Goldstone propagator. Therefore they correspond to terms with  $\tilde{x}$ - and  $\tilde{y}$ -type coefficients respectively.

Following the above rules in analysing the quark flavour flow structure, the results for the baryon sunset diagrams

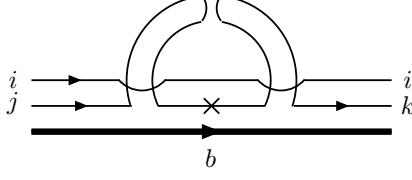


FIG. 9: Quark flavour flow structure for the baryon sunset diagrams with the “hairpin” structure in which the spectator quark (flavour  $i$ ) is absent. The thick line represents the  $b$  quark, and the thin lines are the valence light quarks. The cross is the current  $J_{jk}$ . These diagrams lead to the  $\tilde{y}$  (internal  $S_{ij}$  and  $S_{ik}$  baryons),  $\tilde{y}'$  (internal  $T_{ij}$  and  $S_{ik}$  baryon) and  $\tilde{y}''$  (internal  $S_{ij}$  and  $T_{ik}$  baryons) terms in Eq. (51).

can be written as

$$\begin{aligned}
\mathcal{Q}_{T_{ij} \rightarrow S_{ik}}^{(N_f)} &= g_2^2 \left\{ \sum_a \left[ x_{T_{ij}, S_{ik}, a}^{(N_f)} \mathcal{K}(M_{i,a}, \Delta^{(B)} + \delta_{aj,ij}^{(B)}, \Delta^{(B)} + \delta_{ak,ij}^{(B)}) + \tilde{x}_{T_{ij}, S_{ik}, a}^{(N_f)} \tilde{\mathcal{K}}_{N_f}(M_{i,a}, \Delta^{(B)}, \Delta^{(B)} + \delta_{ik,ij}^{(B)}) \right] \right. \\
&\quad \left. + \tilde{y}_{T_{ij}, S_{ik}}^{(N_f)} \tilde{\mathcal{K}}_{N_f}(M_{j,k}, \Delta^{(B)}, \Delta^{(B)} + \delta_{ik,ij}^{(B)}) \right\} \\
&+ g_3^2 \left\{ \sum_a \left[ x_{T_{ij}, S_{ik}, a}^{\prime(N_f)} \mathcal{K}(M_{i,a}, \Delta^{(B)} + \delta_{aj,ij}^{(B)}, \delta_{ak,ij}^{(B)}) + \tilde{x}_{T_{ij}, S_{ik}, a}^{\prime(N_f)} \tilde{\mathcal{K}}_{N_f}(M_{i,a}, \Delta^{(B)}, \delta_{ik,ij}^{(B)}) \right] \right. \\
&\quad \left. + \tilde{y}_{T_{ij}, S_{ik}}^{\prime(N_f)} \tilde{\mathcal{K}}_{N_f}(M_{j,k}, \Delta^{(B)}, \delta_{ik,ij}^{(B)}) \right\}, \\
\mathcal{Q}_{S_{ij} \rightarrow S_{ik}}^{(N_f)} &= g_2^2 \left\{ \sum_a \left[ x_{S_{ij}, S_{ik}, a}^{(N_f)} \mathcal{K}(M_{i,a}, \delta_{aj,ij}^{(B)}, \delta_{ak,ij}^{(B)}) + \tilde{x}_{S_{ij}, S_{ik}, a}^{(N_f)} \tilde{\mathcal{K}}_{N_f}(M_{i,a}, 0, \delta_{ik,ij}^{(B)}) \right] + \tilde{y}_{S_{ij}, S_{ik}}^{(N_f)} \tilde{\mathcal{K}}_{N_f}(M_{j,k}, 0, \delta_{ik,ij}^{(B)}) \right\} \\
&+ g_3^2 \left\{ \sum_a \left[ x_{S_{ij}, S_{ik}, a}^{\prime(N_f)} \mathcal{K}(M_{i,a}, -\Delta^{(B)} + \delta_{aj,ij}^{(B)}, \delta_{ak,ij}^{(B)}) + \tilde{x}_{S_{ij}, S_{ik}, a}^{\prime(N_f)} \tilde{\mathcal{K}}_{N_f}(M_{i,a}, -\Delta^{(B)}, \delta_{ik,ij}^{(B)}) \right] \right. \\
&\quad \left. + \tilde{y}_{S_{ij}, S_{ik}}^{\prime(N_f)} \tilde{\mathcal{K}}_{N_f}(M_{j,k}, -\Delta^{(B)}, \delta_{ik,ij}^{(B)}) \right. \\
&\quad \left. \sum_a \left[ x_{S_{ij}, S_{ik}, a}^{\prime\prime(N_f)} \mathcal{K}(M_{i,a}, \delta_{aj,ij}^{(B)}, -\Delta^{(B)} + \delta_{ak,ij}^{(B)}) + \tilde{x}_{S_{ij}, S_{ik}, a}^{\prime\prime(N_f)} \tilde{\mathcal{K}}_{N_f}(M_{i,a}, 0, -\Delta^{(B)} + \delta_{ik,ij}^{(B)}) \right] \right. \\
&\quad \left. + \tilde{y}_{S_{ij}, S_{ik}}^{\prime\prime(N_f)} \tilde{\mathcal{K}}_{N_f}(M_{j,k}, 0, -\Delta^{(B)} + \delta_{ik,ij}^{(B)}) \right\}, \tag{51}
\end{aligned}$$

where the summations are over the flavours  $u$  and  $u'$  in the SU(4|2) theory, and are over the flavours  $u$ ,  $s$ ,  $u'$  and  $s'$  in the SU(6|3) theory. The relevant coefficients are presented in Tables IV, V, VI, VII, VIII, IX, and X in Appendix D.

## VI. $H_1 \rightarrow H_2 \pi(K)$ TRANSITION AMPLITUDES

The axial-current matrix elements, presented in the previous sections, are closely related to those in the strong-decay amplitudes, such as

$$\begin{aligned}
B_d^* &\rightarrow B_u \pi, \quad B_s^* \rightarrow B_u K, \\
\Sigma_b^{(*)} &\rightarrow \Lambda_b \pi, \\
\Sigma_b^* &\rightarrow \Sigma_b \pi. \tag{52}
\end{aligned}$$

Note that, with the exception of  $\Sigma_b^{(*)} \rightarrow \Lambda_b \pi$ , for bottom hadrons the above decays are kinematically forbidden in nature. In HH $\chi$ PT, the LO and NLO analytic terms for these decay amplitudes have the same structure as the matrix

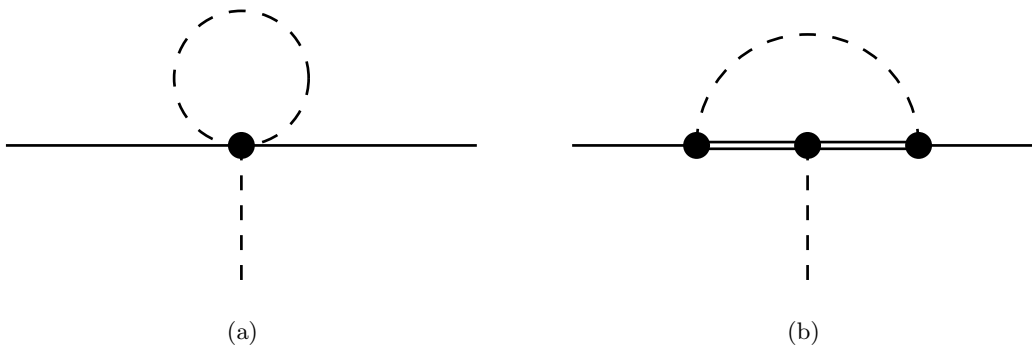


FIG. 10: Diagrams contributing to the decay amplitudes in Eq. (52). The self-energy diagrams leading to wavefunction renormalisation of the external particles are not shown in this figure. The dashed lines are the Goldstone mesons. The single solid lines denote generically the external heavy hadrons, while the double solid lines are the internal heavy hadrons. They can be  $B$ ,  $B^*$  mesons or  $T_{ij}$ ,  $S_{ij}$  baryons. The vertices are all from the axial-coupling terms proportional to  $g_{1,2,3}$  in the strong chiral Lagrangian in Eq. (24). Diagrams (a) and (b) are the “tadpole” and “sunset” types respectively.

elements in Eq. (32). That is, the LO contributions are all proportional to the axial couplings  $g_{1,2,3}$ , while the NLO results are polynomials in the Goldstone masses. Therefore we only address the one-loop diagrams for these decays.

To compute the one-loop amplitudes for the processes in Eq. (52), one has to calculate the wavefunction renormalisation of the Goldstone bosons and the heavy hadrons, as well as the tadpole and sunset diagrams in Fig. 10. The Goldstone boson wavefunction renormalisation can be found in standard references such as [6] and [20], and the heavy hadron wavefunction renormalisation is presented in Eqs. (47) and (48). The amplitudes from the sunset diagram in Fig. 10 (b) are identical to those from the corresponding diagram in Fig. 1 (c). Therefore they are equal to the results presented in Eqs. (49) and (51). The tadpole diagram in Fig. 10 (a) differs from that of the axial-current matrix elements in Fig. 1 (b) by a factor of one-third. That is, one can take the results in Eq. (46), and multiply them by  $1/3$  to obtain the corresponding tadpole-diagram contributions to the decay amplitudes in Eq. (52). It turns out that the contribution from the tadpole diagram is exactly cancelled by the contribution from the wavefunction renormalization of the external Goldstone boson [36]. As is shown in Fig. 2, the tadpole diagrams provide significant contributions to the axial current matrix elements and will lead to significant differences between the quark-mass dependence of axial current matrix elements and that of strong decay amplitudes.

These decay amplitudes have also been computed in Ref. [36], to one-loop order in  $SU(3)$   $HH\chi$ PT in the infinite-volume limit with  $\Delta^{(M)} = \Delta^{(B)} = 0$ , and without the  $SU(3)$  breaking effects from the Lagrangian in Eq. (26). Our results agree with those presented in Ref. [36] in the same limits.

## VII. CONCLUSION

With the expectation of precise data from the LHCb collaboration and from the potential SuperB experiment, accurate QCD calculations of quantities involving  $B$  mesons and single- $b$  baryons will be important in further constraining flavour physics and in looking for physics beyond the SM. This is a challenging but necessary task. In this paper, we have presented calculations for axial-current matrix elements involving single heavy hadron external states in  $HH\chi$ PT at the NLO. We have performed these computations in partially quenched  $\chi$ PT for both  $N_f = 2$  and  $N_f = 2 + 1$ , including finite volume effects. Our results are essential for extracting the axial couplings in  $HH\chi$ PT from experimental data or lattice QCD. These axial couplings are central quantities in  $b$  physics, as they control the light quark mass dependence of  $b$ -hadron observables and determine the strong decay widths of heavy hadrons.

We have discussed the  $SU(2)$  case in detail, numerically analysing the behaviour of the various loop contributions for natural values of the low-energy constants. Based on our study, we conclude that the  $SU(2)$  chiral expansion of the axial current matrix elements is well-behaved for  $M_\pi \lesssim 400$  MeV. This implies that lattice calculations that are performed in this regime can be used to determine the axial couplings reliably.

### Acknowledgments

We warmly thank Brian Tiburzi, André Walker-Loud and Matthew Wingate for helpful discussions. This work is supported by U.S. DoE contract number DE-AC05-06OR-23177, grant number DE-SC000-1784, Jeffress Memorial Trust grant number J-968, and Taiwanese NSC grant number 99-2112-M-009-004-MY3. We acknowledge the hospitality of Academia Sinica Taipei, The College of William and Mary, Thomas Jefferson National Accelerator Facility, National Centre of Theoretical Sciences and National Chiao-Tung University.

### Appendix A: Mass parameters

In this appendix, we define various quantities appearing in our results. First we present the hadron masses,

$$\begin{aligned}
M_{a,b}^2 &= B_0(m_a + m_b), \quad \tilde{\delta}_{VS}^2 = M_{u,u}^2 - M_{u,u'}^2, \quad \tilde{\delta}_{VSs}^2 = M_{s,s}^2 - M_{s,s'}^2, \quad M_X^2 = \frac{1}{3} \left( M_{u,u}^2 + 2M_{s,s}^2 - 2\tilde{\delta}_{VS}^2 - 4\tilde{\delta}_{VSs}^2 \right), \\
\Delta^{(M)} &= M_{B_a^*} - M_{B_b}, \quad \delta_{a,b}^{(M)} = M_{B_a} - M_{B_b} = M_{B_a^*} - M_{B_b^*}, \\
\Delta^{(B)} &= M_{S_{ab}} - M_{T_{ab}}, \quad \delta_{ab,cd}^{(B)} = M_{T_{ab}} - M_{T_{cd}} = M_{S_{ab}} - M_{S_{cd}},
\end{aligned} \tag{A1}$$

where  $B_0$  is defined in Eq. (6). As explained in the main text,  $\Delta^{(M)}$  vanishes in the heavy quark limit, while  $\Delta^{(B)}$  remains non-zero and is of  $O(\Lambda_{\text{QCD}})$ . In this paper, we work in the isospin limit, and denote the pion mass as  $M_{u,u}$ .

It is useful to define the following quantities which appear in the ‘‘hairpin’’ contributions to the flavour-singlet meson propagators in the SU(6|3) theory.

$$\begin{aligned}
A_{u,u} &= \frac{2 \left( \tilde{\delta}_{VS}^2 - M_{u,u}^2 + M_X^2 \right) \tilde{\delta}_{VS}^2}{\left( M_{u,u}^2 - M_X^2 \right)^2} + \frac{3}{2}, \quad A_{s,s} = \frac{3 \left( 8\tilde{\delta}_{VSs}^4 + \left( 2\tilde{\delta}_{VS}^2 - M_{u,u}^2 + M_{s,s}^2 \right)^2 \right)}{\left( 2\tilde{\delta}_{VS}^2 + 4\tilde{\delta}_{VSs}^2 - M_{u,u}^2 + M_{s,s}^2 \right)^2}, \\
C_{u,u} &= 3\tilde{\delta}_{VS}^2 - \frac{2\tilde{\delta}_{VS}^4}{M_{u,u}^2 - M_X^2}, \quad C_{s,s} = \frac{6\tilde{\delta}_{VSs}^2 \left( 2\tilde{\delta}_{VS}^2 - M_{u,u}^2 + M_{s,s}^2 \right)}{2\tilde{\delta}_{VS}^2 + 4\tilde{\delta}_{VSs}^2 - M_{u,u}^2 + M_{s,s}^2}, \\
D_{u,s}^{(u)} &= \frac{2\tilde{\delta}_{VS}^2 \left( M_{u,u}^2 - M_{s,s}^2 + 2\tilde{\delta}_{VSs}^2 \right)}{\left( M_{u,u}^2 - M_{s,s}^2 \right) \left( M_{u,u}^2 - M_X^2 \right)}, \quad D_{u,s}^{(s)} = \frac{2\tilde{\delta}_{VSs}^2 \left( M_{u,u}^2 - M_{s,s}^2 - 2\tilde{\delta}_{VS}^2 \right)}{\left( M_{u,u}^2 - M_{s,s}^2 \right) \left( M_{s,s}^2 - M_X^2 \right)}, \\
D_{u,s}^{(X)} &= \frac{\left( M_{u,u}^2 - M_X^2 - 2\tilde{\delta}_{VS}^2 \right) \left( M_{s,s}^2 - M_X^2 - 2\tilde{\delta}_{VSs}^2 \right)}{\left( M_{u,u}^2 - M_X^2 \right) \left( M_{s,s}^2 - M_X^2 \right)}.
\end{aligned} \tag{A2}$$

In the full QCD limit, where  $m_{u'} = m_u$  and  $m_{s'} = m_s$ ,

$$\begin{aligned}
A_{u,u}^{\text{QCD}} &= \frac{3}{2}, \quad A_{s,s}^{\text{QCD}} = 3, \quad C_{u,u}^{\text{QCD}} = 0, \quad C_{s,s}^{\text{QCD}} = 0, \\
D_{u,s}^{(u)\text{QCD}} &= 0, \quad D_{u,s}^{(s)\text{QCD}} = 0, \quad D_{u,s}^{(X)\text{QCD}} = 1.
\end{aligned} \tag{A3}$$

### Appendix B: Integrals and sums

In this appendix, we present results of loop integrals and sums using dimensional regularisation, with the ultra-violet divergences removed by subtracting the term,

$$\bar{\lambda} = \frac{2}{4-d} - \gamma_E + \log(4\pi) + 1, \quad (\text{B1})$$

where  $d$  is the number of space-time dimensions. This is a commonly-used scheme in  $\chi$ PT calculations [28]. It is different from the  $\overline{\text{MS}}$  scheme by the constant “1” on the right-hand side of the above equation. It can also be changed into the scheme discussed in Sec. IV A straightforwardly. Finite volume effects in the limit  $mL \gg 1$  ( $m$  is a generic Goldstone mass and  $L$  is the spatial lattice volume) are computed by replacing the momentum integrals by sums in the spatial directions. The one-loop contributions appearing in this work can all be obtained by investigating the following sums/integrals

$$\begin{aligned} \mathcal{I}(m) &\equiv \mu^{4-d} \sum \int \frac{d^d k}{(2\pi)^d} \frac{i}{k^2 - m^2 + i\epsilon} - \frac{m^2}{16\pi^2} \bar{\lambda}, \\ \mathcal{F}(m, \Delta) &\equiv (g^{\rho\nu} - v^\rho v^\nu) \left[ \frac{\mu^{4-d}}{(d-1)} \sum \int \frac{d^d k}{(2\pi)^d} \frac{ik_\rho k_\nu}{(k^2 - m^2 + i\epsilon)(v \cdot k - \Delta + i\epsilon)} + \frac{g_{\rho\nu}}{16\pi^2} \bar{\lambda} \left( \frac{2\Delta^2}{3} - m^2 \right) \Delta \right], \end{aligned} \quad (\text{B2})$$

where  $\mu$  is the renormalisation scale, and the symbol

$$\sum \int d^d k$$

means performing the sums in three spatial directions using the Poisson summation formula, followed by dimensionally regularising the infinite-volume integrals.

We can further separate the infinite-volume limit of  $\mathcal{I}$  and  $\mathcal{F}$  from the finite-volume contributions,

$$\begin{aligned} \mathcal{I}(m) &= I(m) + I_{\text{FV}}(m), \\ \mathcal{F}(m) &= F(m, \Delta) + F_{\text{FV}}(m). \end{aligned} \quad (\text{B3})$$

The functions  $I$  and  $F$  are results from the ordinary one-loop integrals,

$$\begin{aligned} I(m) &= \frac{m^2}{16\pi^2} \log \left( \frac{m^2}{\mu^2} \right), \\ F(m, \Delta) &= \frac{-1}{16\pi^2} \left[ \left( m^2 - \frac{2\Delta^2}{3} \right) \Delta \log \left( \frac{m^2}{\mu^2} \right) + \left( \frac{10\Delta^2}{9} - \frac{4m^2}{3} \right) \Delta + \frac{2(\Delta^2 - m^2)}{3} m R \left( \frac{\Delta}{m} \right) \right], \end{aligned} \quad (\text{B4})$$

with

$$R(x) \equiv \sqrt{x^2 - 1} \left[ \log \left( x - \sqrt{x^2 - 1 + i\epsilon} \right) - \log \left( x + \sqrt{x^2 - 1 + i\epsilon} \right) \right]. \quad (\text{B5})$$

The function  $F(m, \Delta)$  does not vanish in the  $m \rightarrow 0$  limit unless  $\Delta = 0$ . One can adopt the scheme discussed in Sec. IV A by simply rewriting  $F$  as  $F^{(\text{sub})}$  defined in Eq. (43), and the real part of the function  $F^{(\text{sub})}$  is zero in the chiral limit for arbitrary  $\Delta$ .

For the case in which the external hadrons are stable particles, the finite-volume pieces can be shown to be [9, 37]<sup>11</sup>

$$\begin{aligned}
I_{\text{FV}}(m) &= \frac{m}{4\pi^2} \sum_{\vec{u} \neq \vec{0}} \frac{1}{uL} K_1(umL) \\
&\xrightarrow{mL \gg 1} \frac{1}{4\pi^2} \sum_{\vec{u} \neq \vec{0}} \sqrt{\frac{m\pi}{2uL}} \left(\frac{1}{uL}\right) e^{-umL} \times \left\{ 1 + \frac{3}{8umL} - \frac{15}{128(umL)^2} + \mathcal{O}\left(\left[\frac{1}{umL}\right]^3\right) \right\}, \\
F_{\text{FV}}(m, \Delta) &= \frac{-1}{12\pi^2} \sum_{\vec{u} \neq \vec{0}} \frac{1}{uL} \int_0^\infty d|\vec{k}| \frac{|\vec{k}| \sin(u|\vec{k}|L)}{\sqrt{|\vec{k}|^2 + m^2 + \Delta}} \left( \Delta + \frac{m^2}{\sqrt{|\vec{k}|^2 + m^2}} \right) \\
&\xrightarrow{mL \gg 1} \frac{-m^2}{24\pi} \sum_{\vec{u} \neq \vec{0}} \frac{e^{-umL}}{uL} \mathcal{A}, \tag{B6}
\end{aligned}$$

where  $\vec{u} = (u_1, u_2, u_3)$  with  $u_i \in \mathbb{Z}$ ,  $u \equiv |\vec{u}|$  and

$$\begin{aligned}
\mathcal{A} &= e^{(z^2)} [1 - \text{Erf}(z)] + \left(\frac{1}{umL}\right) \left[ \frac{1}{\sqrt{\pi}} \left(\frac{9z}{4} - \frac{z^3}{2}\right) + \left(\frac{z^4}{2} - 2z^2\right) e^{(z^2)} [1 - \text{Erf}(z)] \right] \\
&\quad - \left(\frac{1}{umL}\right)^2 \left[ \frac{1}{\sqrt{\pi}} \left(-\frac{39z}{64} + \frac{11z^3}{32} - \frac{9z^5}{16} + \frac{z^7}{8}\right) - \left(-\frac{z^6}{2} + \frac{z^8}{8}\right) e^{(z^2)} [1 - \text{Erf}(z)] \right] + \mathcal{O}\left(\frac{1}{(umL)^3}\right), \tag{B7}
\end{aligned}$$

with

$$z = \left(\frac{\Delta}{m}\right) \sqrt{\frac{umL}{2}}. \tag{B8}$$

Higher order terms in the  $1/(umL)$  expansion in Eq. (B7) can be easily calculated. The integer  $u_i$  can be interpreted as the number of times that the pion wraps around the spatial volume in the  $i$ -the direction.

The functions appearing in our one-loop results are

$$\begin{aligned}
\mathcal{H}(m, \Delta) &\equiv \frac{\partial \mathcal{F}(m, \Delta)}{\partial \Delta} \quad \text{and} \quad \mathcal{K}(m, \Delta_1, \Delta_2) \equiv \frac{\mathcal{F}(m, \Delta_1) - \mathcal{F}(m, \Delta_2)}{\Delta_1 - \Delta_2}, \\
\mathcal{I}_{\eta'}(m) &\equiv \frac{\partial \mathcal{I}(m)}{\partial m^2}, \quad \mathcal{H}_{\eta'}(m, \Delta) \equiv \frac{\partial \mathcal{H}(m, \Delta)}{\partial m^2} \quad \text{and} \quad \mathcal{K}_{\eta'}(m, \Delta_1, \Delta_2) \equiv \frac{\partial \mathcal{K}(m, \Delta_1, \Delta_2)}{\partial m^2}. \tag{B9}
\end{aligned}$$

Notice that

$$\mathcal{K}(m, \Delta, \Delta) \equiv \lim_{\Delta' \rightarrow \Delta} \mathcal{K}(m, \Delta, \Delta') = \mathcal{H}(m, \Delta). \tag{B10}$$

To present the residual flavour-singlet ‘‘hairpin’’ contributions in a compact form, we define three functions

$$\tilde{\mathcal{I}}_{N_f}(m), \quad \tilde{\mathcal{H}}_{N_f}(m, \Delta), \quad \text{and} \quad \tilde{\mathcal{K}}_{N_f}(m, \Delta_1, \Delta_2). \tag{B11}$$

They take the explicit form

$$\begin{aligned}
\tilde{\mathcal{I}}_2(m) &= \mathcal{I}(m) + 2\tilde{\delta}_{V_S}^2 \mathcal{I}_{\eta'}(m), \\
\tilde{\mathcal{H}}_2(m, \Delta) &= \mathcal{H}(m, \Delta) + 2\tilde{\delta}_{V_S}^2 \mathcal{H}_{\eta'}(m, \Delta), \\
\tilde{\mathcal{K}}_2(m, \Delta_1, \Delta_2) &= \mathcal{K}(m, \Delta_1, \Delta_2) + 2\tilde{\delta}_{V_S}^2 \mathcal{K}_{\eta'}(m, \Delta_1, \Delta_2), \tag{B12}
\end{aligned}$$

<sup>11</sup> Similar formulae for finite-volume effects are also obtained in Ref. [38].

$a$	$u$	$s$	$u'$	$s'$
$w_{B_u,a}^{(2)}$	0	0	3	0
$\tilde{w}_{B_u,a}^{(2)}$	$-\frac{3}{4}$	0	0	0
$w_{B_u,a}^{(3)}$	0	0	3	$\frac{3}{2}$
$\tilde{w}_{B_u,a}^{(3)}$	$-\frac{1}{2}$	0	0	0
$w_{B_d^*,a}^{(2)}$	0	0	1	0
$\tilde{w}_{B_d^*,a}^{(2)}$	$-\frac{1}{4}$	0	0	0
$w_{B_d^*,a}^{(2)}$	0	0	2	0
$\tilde{w}_{B_d^*,a}^{(2)}$	$-\frac{1}{2}$	0	0	0
$w_{B_d^*,a}^{(3)}$	0	0	1	$\frac{1}{2}$
$\tilde{w}_{B_d^*,a}^{(3)}$	$-\frac{1}{6}$	0	0	0
$w_{B_d^*,a}^{(3)}$	0	0	2	1
$\tilde{w}_{B_d^*,a}^{(3)}$	$-\frac{1}{3}$	0	0	0
$w_{B_s^*,a}^{(3)}$	0	0	1	$\frac{1}{2}$
$\tilde{w}_{B_s^*,a}^{(3)}$	0	$-\frac{1}{6}$	0	0
$w_{B_s^*,a}^{(3)}$	0	0	2	1
$\tilde{w}_{B_s^*,a}^{(3)}$	0	$-\frac{1}{3}$	0	0

TABLE I: Coefficients for heavy-light meson wavefunction renormalisation, in Eqs. (47), in the isospin limit.

in the SU(4|2) theory ( $N_f = 2$ ) where the mass  $m$  in the arguments is always equal to  $M_{u,u}$ , and

$$\begin{aligned} \tilde{\mathcal{I}}_3(M_{a,b}) &= \delta_{a,b} \{A_{a,b} \mathcal{I}(M_{a,b}) + (1 - A_{a,b}) \mathcal{I}(M_X) + C_{a,b} \mathcal{I}_{\eta'}(M_{a,b})\} \\ &+ (1 - \delta_{a,b}) \left\{ D_{a,b}^{(a)} \mathcal{I}(M_{a,a}) + D_{a,b}^{(b)} \mathcal{I}(M_{b,b}) + D_{a,b}^{(X)} \mathcal{I}(M_X) \right\}, \end{aligned}$$

$$\begin{aligned} \tilde{\mathcal{H}}_3(M_{a,b}, \Delta) &= \delta_{a,b} \{A_{a,b} \mathcal{H}(M_{a,b}, \Delta) + (1 - A_{a,b}) \mathcal{H}(M_X, \Delta) + C_{a,b} \mathcal{H}_{\eta'}(M_{a,b}, \Delta)\} \\ &+ (1 - \delta_{a,b}) \left\{ D_{a,b}^{(a)} \mathcal{H}(M_{a,a}, \Delta) + D_{a,b}^{(b)} \mathcal{H}(M_{b,b}, \Delta) + D_{a,b}^{(X)} \mathcal{H}(M_X, \Delta) \right\}, \end{aligned}$$

$$\begin{aligned} \tilde{\mathcal{K}}_3(M_{a,b}, \Delta_1, \Delta_2) &= \delta_{a,b} \{A_{a,b} \mathcal{K}(M_{a,b}, \Delta_1, \Delta_2) + (1 - A_{a,b}) \mathcal{K}(M_X, \Delta_1, \Delta_2) + C_{a,b} \mathcal{K}_{\eta'}(M_{a,b}, \Delta_1, \Delta_2)\} \\ &+ (1 - \delta_{a,b}) \left\{ D_{a,b}^{(a)} \mathcal{K}(M_{a,a}, \Delta_1, \Delta_2) + D_{a,b}^{(b)} \mathcal{K}(M_{b,b}, \Delta_1, \Delta_2) + D_{a,b}^{(X)} \mathcal{K}(M_X, \Delta_1, \Delta_2) \right\}, \end{aligned} \quad (\text{B13})$$

in the SU(6|3) theory ( $N_f = 3$ ).

### Appendix C: Coefficients for wavefunction renormalisation

In this Appendix, we present the coefficients in Eqs. (47) and (48) relevant to the matrix elements investigated in this work. These coefficients are summarised in Tables I, II and III. Because of isospin symmetry, it is not possible (or necessary) to distinguish between the  $w$  and  $u$  coefficients for some of the hadrons in the current study. For such cases, we simply present  $w + u$  in the tables.

$a$	$u$	$s$	$u'$	$s'$
$w_{T_{du,a}}^{(2)} + u_{T_{du,a}}^{(2)}$	$\frac{3}{2}$	0	3	0
$\tilde{w}_{T_{du,a}}^{(2)} + \tilde{u}_{T_{du,a}}^{(2)}$	0	0	0	0
$w_{T_{du,a}}^{(3)} + u_{T_{du,a}}^{(3)}$	$\frac{3}{2}$	0	3	$\frac{3}{2}$
$\tilde{w}_{T_{du,a}}^{(3)} + \tilde{u}_{T_{du,a}}^{(3)}$	0	0	0	0
$w_{T_{su,a}}^{(3)}$	0	$\frac{3}{4}$	$\frac{3}{2}$	$\frac{3}{4}$
$\tilde{w}_{T_{su,a}}^{(3)}$	$-\frac{1}{4}$	0	0	0
$u_{T_{su,a}}^{(3)}$	$\frac{3}{4}$	0	$\frac{3}{2}$	$\frac{3}{4}$
$\tilde{u}_{T_{su,a}}^{(3)}$	$\frac{1}{2}$	$-\frac{1}{4}$	0	0

TABLE II: Coefficients for  $T_{ij}$  baryon wavefunction renormalisation, in Eq. (48), in the isospin limit.

$a$	$u$	$s$	$u'$	$s'$
$w_{S_{du,a}}^{\prime(2)} + u_{S_{du,a}}^{\prime(2)}$	$-\frac{1}{2}$	0	1	0
$\tilde{w}_{S_{du,a}}^{\prime(2)} + \tilde{u}_{S_{du,a}}^{\prime(2)}$	0	0	0	0
$w_{S_{du,a}}^{(2)} + u_{S_{du,a}}^{(2)}$	$\frac{1}{2}$	0	1	0
$\tilde{w}_{S_{du,a}}^{(2)} + \tilde{u}_{S_{du,a}}^{(2)}$	$-\frac{1}{2}$	0	0	0
$w_{S_{du,a}}^{\prime(3)} + u_{S_{du,a}}^{\prime(3)}$	$-\frac{1}{2}$	0	1	$\frac{1}{2}$
$\tilde{w}_{S_{du,a}}^{\prime(3)} + \tilde{u}_{S_{du,a}}^{\prime(3)}$	0	0	0	0
$w_{S_{du,a}}^{(3)} + u_{S_{du,a}}^{(3)}$	$\frac{1}{2}$	0	1	$\frac{1}{2}$
$\tilde{w}_{S_{du,a}}^{(3)} + \tilde{u}_{S_{du,a}}^{(3)}$	$-\frac{1}{3}$	0	0	0
$w_{S_{su,a}}^{\prime(3)}$	0	$-\frac{1}{4}$	$\frac{1}{2}$	$\frac{1}{4}$
$\tilde{w}_{S_{su,a}}^{\prime(3)}$	$-\frac{1}{12}$	0	0	0
$u_{S_{su,a}}^{\prime(3)}$	$-\frac{1}{4}$	0	$\frac{1}{2}$	$\frac{1}{4}$
$\tilde{u}_{S_{su,a}}^{\prime(3)}$	$\frac{1}{6}$	$-\frac{1}{12}$	0	0
$w_{S_{su,a}}^{(3)}$	0	$\frac{1}{4}$	$\frac{1}{2}$	$\frac{1}{4}$
$\tilde{w}_{S_{su,a}}^{(3)}$	$-\frac{1}{12}$	0	0	0
$u_{S_{su,a}}^{(3)}$	$\frac{1}{4}$	0	$\frac{1}{2}$	$\frac{1}{4}$
$\tilde{u}_{S_{su,a}}^{(3)}$	$-\frac{1}{6}$	$-\frac{1}{12}$	0	0
$w_{S_{ss,a}}^{\prime(3)} + u_{S_{ss,a}}^{\prime(3)}$	0	$-\frac{1}{2}$	1	$\frac{1}{2}$
$\tilde{w}_{S_{ss,a}}^{\prime(3)} + \tilde{u}_{S_{ss,a}}^{\prime(3)}$	0	0	0	0
$w_{S_{ss,a}}^{(3)} + u_{S_{ss,a}}^{(3)}$	0	$\frac{1}{2}$	1	$\frac{1}{2}$
$\tilde{w}_{S_{ss,a}}^{(3)} + \tilde{u}_{S_{ss,a}}^{(3)}$	0	$-\frac{1}{3}$	0	0

TABLE III: Coefficients for  $S_{ij}$  baryon wavefunction renormalisation, in Eq. (48), in the isospin limit.

#### Appendix D: Coefficients for the sunset diagrams

In this Appendix, we present the coefficients in Eqs. (49) and (51) relevant to the matrix elements investigated in this work. Because of the isospin symmetry, it is impossible to distinguish between some  $\tilde{y}$  coefficients and their  $\tilde{x}$  counterparts. For such cases, we put the symbol  $+\tilde{x}$  in Table VII, and then present  $\tilde{x} + \tilde{y}$  in Tables VIII, IX and X in the form that  $\tilde{x}$  is written as (number -  $\tilde{y}$ ).

$a$	$u$	$s$	$u'$	$s'$
$x_{T_{du},S_{dd},a}^{(2)}$	-1	0	-1	0
$x_{T_{du},S_{dd},a}^{(3)}$	-1	0	-1	$-\frac{1}{2}$
$x_{T_{su},S_{sd},a}^{(3)}$	-1	0	-1	$-\frac{1}{2}$
$x_{T_{du},S_{ds},a}^{(3)}$	$-\frac{1}{2}$	$-\frac{1}{2}$	-1	$-\frac{1}{2}$
$x_{T_{su},S_{ss},a}^{(3)}$	$-\frac{1}{2}$	$-\frac{1}{2}$	-1	$-\frac{1}{2}$
$x_{S_{du},S_{dd},a}^{(2)}$	$-\frac{1}{2}$	0	$-\frac{1}{2}$	0
$x_{S_{du},S_{dd},a}^{(3)}$	$-\frac{1}{2}$	0	$-\frac{1}{2}$	$-\frac{1}{4}$
$x_{S_{su},S_{sd},a}^{(3)}$	$-\frac{1}{2}$	0	$-\frac{1}{2}$	$-\frac{1}{4}$
$x_{S_{du},S_{ds},a}^{(3)}$	$-\frac{1}{4}$	$-\frac{1}{4}$	$-\frac{1}{2}$	$-\frac{1}{4}$
$x_{S_{su},S_{ss},a}^{(3)}$	$-\frac{1}{4}$	$-\frac{1}{4}$	$-\frac{1}{2}$	$-\frac{1}{4}$

TABLE IV: Coefficients  $x_{H_1,H_2}^{(N_f)}$  in Eq. (51), in the isospin limit.

$a$	$u$	$s$	$u'$	$s'$
$x_{S_{du},S_{dd},a}^{\prime(2)}$	0	0	-1	0
$x_{S_{du},S_{dd},a}^{\prime(3)}$	0	0	-1	$-\frac{1}{2}$
$x_{S_{su},S_{sd},a}^{\prime(3)}$	0	0	-1	$-\frac{1}{2}$
$x_{S_{du},S_{ds},a}^{\prime(3)}$	$\frac{1}{2}$	$-\frac{1}{2}$	-1	$-\frac{1}{2}$
$x_{S_{su},S_{ss},a}^{\prime(3)}$	$\frac{1}{2}$	$-\frac{1}{2}$	-1	$-\frac{1}{2}$

TABLE V: Coefficients  $x_{H_1,H_2}^{\prime(N_f)}$  in Eq. (51), in the isospin limit.

$a$	$u$	$s$	$u'$	$s'$
$x_{T_{du},S_{dd},a}^{\prime\prime(2)}$	0	0	-1	0
$x_{T_{du},S_{dd},a}^{\prime\prime(3)}$	0	0	-1	$-\frac{1}{2}$
$x_{T_{su},S_{sd},a}^{\prime\prime(3)}$	0	0	-1	$-\frac{1}{2}$
$x_{T_{du},S_{ds},a}^{\prime\prime(3)}$	$-\frac{1}{2}$	$\frac{1}{2}$	-1	$-\frac{1}{2}$
$x_{T_{su},S_{ss},a}^{\prime\prime(3)}$	$-\frac{1}{2}$	$\frac{1}{2}$	-1	$-\frac{1}{2}$
$x_{S_{du},S_{dd},a}^{\prime\prime(2)}$	0	0	-1	0
$x_{S_{du},S_{dd},a}^{\prime\prime(3)}$	0	0	-1	$-\frac{1}{2}$
$x_{S_{su},S_{sd},a}^{\prime\prime(3)}$	0	0	-1	$-\frac{1}{2}$
$x_{S_{du},S_{ds},a}^{\prime\prime(3)}$	$-\frac{1}{2}$	$\frac{1}{2}$	-1	$-\frac{1}{2}$
$x_{S_{su},S_{ss},a}^{\prime\prime(3)}$	$-\frac{1}{2}$	$\frac{1}{2}$	-1	$-\frac{1}{2}$

TABLE VI: Coefficients  $x_{H_1,H_2}^{\prime\prime(N_f)}$  in Eq. (51), in the isospin limit.

$\tilde{y}_{B_u, B_d^*}^{(2)}$	$\tilde{y}_{B_u, B_d^*}^{(3)}$	$\tilde{y}_{B_u, B_s^*}^{(3)}$	$\tilde{y}_{T_{du}, S_{dd}}^{(2)}$	$\tilde{y}_{T_{du}, S_{dd}}^{(3)}$	$\tilde{y}_{T_{su}, S_{sd}}^{(3)}$	$\tilde{y}_{T_{du}, S_{ds}}^{(3)}$	$\tilde{y}_{T_{su}, S_{ss}}^{(3)}$	$\tilde{y}_{S_{du}, S_{dd}}^{(2)}$	$\tilde{y}_{S_{du}, S_{dd}}^{(3)}$	$\tilde{y}_{S_{su}, S_{sd}}^{(3)}$	$\tilde{y}_{S_{du}, S_{ds}}^{(3)}$	$\tilde{y}_{S_{su}, S_{ss}}^{(3)}$
-1	$-\frac{2}{3}$	$-\frac{2}{3}$	$+\tilde{x}$	$+\tilde{x}$	$-\frac{1}{6}$	$+\tilde{x}$	$+\tilde{x}$	$+\tilde{x}$	$+\tilde{x}$	$\frac{1}{12}$	$+\tilde{x}$	$+\tilde{x}$
$\tilde{y}'_{B_u, B_d^*}{}^{(2)}$	$\tilde{y}'_{B_u, B_d^*}{}^{(3)}$	$\tilde{y}'_{B_u, B_s^*}{}^{(3)}$	$\tilde{y}'_{S_{du}, S_{dd}}{}^{(2)}$	$\tilde{y}'_{S_{du}, S_{dd}}{}^{(3)}$	$\tilde{y}'_{S_{su}, S_{sd}}{}^{(3)}$	$\tilde{y}'_{S_{du}, S_{ds}}{}^{(3)}$	$\tilde{y}'_{S_{su}, S_{ss}}{}^{(3)}$					
$\frac{1}{2}$	$\frac{1}{3}$	$\frac{1}{3}$	$+\tilde{x}'$	$+\tilde{x}'$	$-\frac{1}{6}$	$+\tilde{x}'$	$+\tilde{x}'$					
$\tilde{y}''_{T_{du}, S_{dd}}{}^{(2)}$	$\tilde{y}''_{T_{du}, S_{dd}}{}^{(3)}$	$\tilde{y}''_{T_{su}, S_{sd}}{}^{(3)}$	$\tilde{y}''_{T_{du}, S_{ds}}{}^{(3)}$	$\tilde{y}''_{T_{su}, S_{ss}}{}^{(3)}$	$\tilde{y}''_{S_{du}, S_{dd}}{}^{(2)}$	$\tilde{y}''_{S_{du}, S_{dd}}{}^{(3)}$	$\tilde{y}''_{S_{su}, S_{sd}}{}^{(3)}$	$\tilde{y}''_{S_{du}, S_{ds}}{}^{(3)}$	$\tilde{y}''_{S_{su}, S_{ss}}{}^{(3)}$			
$+\tilde{x}''$	$+\tilde{x}''$	$\frac{1}{6}$	$+\tilde{x}''$	$+\tilde{x}''$	$+\tilde{x}''$	$+\tilde{x}''$	$+\tilde{x}''$	$-\frac{1}{6}$	$+\tilde{x}''$	$+\tilde{x}''$		

TABLE VII: Coefficients  $\tilde{y}_{H_1, H_2}^{(N_f)}$ ,  $\tilde{y}'_{H_1, H_2}{}^{(N_f)}$  and  $\tilde{y}''_{H_1, H_2}{}^{(N_f)}$  in Eqs. (49) and (51). Due to the isospin symmetry, some of these coefficients cannot be distinguished from their  $\tilde{x}_{H_1, H_2}^{(N_f)}$  counterparts. For such cases, the values are denoted  $+\tilde{x}$  in the table, and are presented together with the corresponding  $\tilde{x}_{H_1, H_2}^{(N_f)}$ .

$a$	$u$	$s$	$u'$	$s'$
$\tilde{x}_{T_{du}, S_{dd}, a}^{(2)}$	$0 - \tilde{y}_{T_{du}, S_{dd}}^{(2)}$	0	0	0
$\tilde{x}_{T_{du}, S_{dd}, a}^{(3)}$	$0 - \tilde{y}_{T_{du}, S_{dd}}^{(3)}$	0	0	0
$\tilde{x}_{T_{su}, S_{sd}, a}^{(3)}$	0	$\frac{1}{6}$	0	0
$\tilde{x}_{T_{du}, S_{ds}, a}^{(3)}$	0	$0 - \tilde{y}_{T_{du}, S_{ds}}^{(3)}$	0	0
$\tilde{x}_{T_{su}, S_{ss}, a}^{(3)}$	$-\frac{1}{3} - \tilde{y}_{T_{su}, S_{ss}}^{(3)}$	$\frac{1}{3}$	0	0
$\tilde{x}_{S_{du}, S_{dd}, a}^{(2)}$	$\frac{1}{2} - \tilde{y}_{S_{du}, S_{dd}}^{(2)}$	0	0	0
$\tilde{x}_{S_{du}, S_{dd}, a}^{(3)}$	$\frac{1}{3} - \tilde{y}_{S_{du}, S_{dd}}^{(3)}$	0	0	0
$\tilde{x}_{S_{su}, S_{sd}, a}^{(3)}$	$\frac{1}{6}$	$\frac{1}{12}$	0	0
$\tilde{x}_{S_{du}, S_{ds}, a}^{(3)}$	$\frac{1}{6}$	$\frac{1}{6} - \tilde{y}_{S_{du}, S_{ds}}^{(3)}$	0	0
$\tilde{x}_{S_{su}, S_{ss}, a}^{(3)}$	$\frac{1}{6} - \tilde{y}_{S_{su}, S_{ss}}^{(3)}$	$\frac{1}{6}$	0	0

TABLE VIII: Coefficients  $\tilde{x}_{H_1, H_2}^{(N_f)}$  in Eq. (51). Due to the isospin symmetry, some of them cannot be distinguished from their  $\tilde{y}_{H_1, H_2}^{(N_f)}$  counterparts. For such cases, we present  $\tilde{x}_{H_1, H_2}^{(N_f)} + \tilde{y}_{H_1, H_2}^{(N_f)}$  in the table.

$a$	$u$	$s$	$u'$	$s'$
$\tilde{x}_{S_{du}, S_{dd}, a}^{(2)}$	$0 - \tilde{y}_{S_{du}, S_{dd}}^{(2)}$	0	0	0
$\tilde{x}_{S_{du}, S_{dd}, a}^{(3)}$	$0 - \tilde{y}_{S_{du}, S_{dd}}^{(3)}$	0	0	0
$\tilde{x}_{S_{su}, S_{sd}, a}^{(3)}$	0	$\frac{1}{6}$	0	0
$\tilde{x}_{S_{du}, S_{ds}, a}^{(3)}$	0	$0 - \tilde{y}_{S_{du}, S_{ds}}^{(3)}$	0	0
$\tilde{x}_{S_{su}, S_{ss}, a}^{(3)}$	$-\frac{1}{3} - \tilde{y}_{S_{su}, S_{ss}}^{(3)}$	$\frac{1}{3}$	0	0

TABLE IX: Coefficients  $\tilde{x}'_{H_1, H_2}{}^{(N_f)}$  in Eq. (51). Due to the isospin symmetry, some of them cannot be distinguished from their  $\tilde{y}'_{H_1, H_2}{}^{(N_f)}$  counterparts. For such cases, we present  $\tilde{x}'_{H_1, H_2}{}^{(N_f)} + \tilde{y}'_{H_1, H_2}{}^{(N_f)}$  in the table.

$a$	$u$	$s$	$u'$	$s'$
$\tilde{x}_{T_{du},S_{dd},a}^{''(2)}$	$0 - \tilde{y}_{T_{du},S_{dd}}^{''(2)}$	0	0	0
$\tilde{x}_{T_{du},S_{dd},a}^{''(3)}$	$0 - \tilde{y}_{T_{du},S_{dd}}^{''(3)}$	0	0	0
$\tilde{x}_{T_{su},S_{sd},a}^{''(3)}$	$\frac{-1}{3}$	$\frac{1}{6}$	0	0
$\tilde{x}_{T_{du},S_{ds},a}^{''(3)}$	0	$0 - \tilde{y}_{T_{du},S_{ds}}^{''(3)}$	0	0
$\tilde{x}_{T_{su},S_{ss},a}^{''(3)}$	$0 - \tilde{y}_{T_{su},S_{ss}}^{''(3)}$	0	0	0
$\tilde{x}_{S_{du},S_{dd},a}^{''(2)}$	$0 - \tilde{y}_{S_{du},S_{dd}}^{''(2)}$	0	0	0
$\tilde{x}_{S_{du},S_{dd},a}^{''(3)}$	$0 - \tilde{y}_{S_{du},S_{dd}}^{''(3)}$	0	0	0
$\tilde{x}_{S_{su},S_{sd},a}^{''(3)}$	0	$\frac{1}{6}$	0	0
$\tilde{x}_{S_{du},S_{ds},a}^{''(3)}$	$\frac{1}{3}$	$\frac{-1}{3} - \tilde{y}_{S_{du},S_{ds}}^{''(3)}$	0	0
$\tilde{x}_{S_{su},S_{ss},a}^{''(3)}$	$0 - \tilde{y}_{S_{su},S_{ss}}^{''(3)}$	0	0	0

TABLE X: Coefficients  $\tilde{x}_{H_1,H_2}^{''(N_f)}$  in Eq. (51). Due to the isospin symmetry, some of them cannot be distinguished from their  $\tilde{y}_{H_1,H_2}^{''(N_f)}$  counterparts. For such cases, we present  $\tilde{x}_{H_1,H_2}^{''(N_f)} + \tilde{y}_{H_1,H_2}^{''(N_f)}$  in the table.

- 
- [1] G. Burdman and J. F. Donoghue, Phys. Lett. **B280**, 287 (1992).
  - [2] M. B. Wise, Phys. Rev. **D45**, 2188 (1992).
  - [3] T.-M. Yan et al., Phys. Rev. **D46**, 1148 (1992), [Erratum-ibid **D55**, 5851 (1997)].
  - [4] P. L. Cho, Phys. Lett. **B285**, 145 (1992), hep-ph/9203225.
  - [5] P. L. Cho, Nucl. Phys. **B396**, 183 (1993), [Erratum-ibid. **B421**, 683 (1994)], hep-ph/9208244.
  - [6] C. W. Bernard and M. F. L. Golterman, Phys. Rev. **D49**, 486 (1994), hep-lat/9306005.
  - [7] F. Bernardoni, P. Hernandez, and S. Necco, JHEP **1001**, 070 (2010), arXiv:0910.2537.
  - [8] R. A. Briceno (2011), arXiv:1108.0120.
  - [9] D. Arndt and C.-J. D. Lin, Phys. Rev. **D70**, 014503 (2004), hep-lat/0403012.
  - [10] W. Detmold and C.-J. D. Lin, Phys. Rev. **D76**, 014501 (2007), hep-lat/0612028.
  - [11] G. Colangelo, A. Fuhrer, and S. Lanz, Phys. Rev. **D82**, 034506 (2010), arXiv:1005.1485.
  - [12] G. de Divitiis et al. (UKQCD Collaboration), JHEP **9810**, 010 (1998), hep-lat/9807032.
  - [13] A. Abada, D. Becirevic, P. Boucaud, G. Herdoiza, J. Leroy, et al., JHEP **0402**, 016 (2004), hep-lat/0310050.
  - [14] H. Ohki, H. Matsufuru, and T. Onogi, Phys. Rev. **D77**, 094509 (2008), arXiv:0802.1563.
  - [15] D. Becirevic, B. Blossier, E. Chang, and B. Haas, Phys. Lett. **B679**, 231 (2009), arXiv:0905.3355.
  - [16] J. Bulava, M. Donnellan, and R. Sommer (ALPHA Collaboration), PoS **LATTICE2010**, 303 (2010), arXiv:1011.4393.
  - [17] J. Bulava, M. Donnellan, and R. Sommer (2011), arXiv:1108.3774.
  - [18] C. W. Bernard and M. F. L. Golterman, Phys. Rev. **D53**, 476 (1996), hep-lat/9507004.
  - [19] S. R. Sharpe and N. Shores, Phys. Rev. **D64**, 114510 (2001), hep-lat/0108003.
  - [20] S. R. Sharpe and N. Shores, Phys. Rev. **D62**, 094503 (2000), hep-lat/0006017.
  - [21] S. R. Sharpe and Y. Zhang, Phys. Rev. **D53**, 5125 (1996), hep-lat/9510037.
  - [22] M. J. Savage, Phys. Rev. **D65**, 034014 (2002), hep-ph/0109190.
  - [23] C. G. Boyd and B. Grinstein, Nucl. Phys. **B442**, 205 (1995), hep-ph/9402340.
  - [24] K. Nakamura et al. (Particle Data Group), J. Phys. **G37**, 075021 (2010).
  - [25] D. Arndt, S. R. Beane, and M. J. Savage, Nucl. Phys. **A726**, 339 (2003), nucl-th/0304004.
  - [26] T. Aaltonen et al. (CDF Collaboration), Phys. Rev. Lett. **99**, 202001 (2007), arXiv:0706.3868.
  - [27] I. W. Stewart, Nucl. Phys. **B529**, 62 (1998), hep-ph/9803227.
  - [28] J. Gasser and H. Leutwyler, Nucl. Phys. **B250**, 465 (1985).
  - [29] B. C. Tiburzi and A. Walker-Loud, Nucl. Phys. **A764**, 274 (2006), hep-lat/0501018.
  - [30] A. Walker-Loud (2006), Ph.D. Thesis, hep-lat/0608010.
  - [31] L. Lellouch and M. Lüscher, Commun. Math. Phys. **219**, 31 (2001), hep-lat/0003023.
  - [32] V. Bernard, U.-G. Meissner, and A. Rusetsky, Nucl. Phys. **B788**, 1 (2008), hep-lat/0702012.
  - [33] W. Detmold, C.-J. D. Lin, and S. Meinel, in preparation.
  - [34] S. R. Sharpe, Phys. Rev. **D46**, 3146 (1992), hep-lat/9205020.
  - [35] B. C. Tiburzi, Phys. Rev. **D71**, 034501 (2005), hep-lat/0410033.
  - [36] H.-Y. Cheng, C.-Y. Cheung, G.-L. Lin, Y. Lin, T.-M. Yan, et al., Phys. Rev. **D49**, 5857 (1994), hep-ph/9312304.
  - [37] W. Detmold and C.-J. D. Lin, Phys. Rev. **D71**, 054510 (2005), hep-lat/0501007.
  - [38] S. R. Beane, Phys. Rev. **D70**, 034507 (2004), hep-lat/0403015.